Atmos. Chem. Phys., 18, 13013–13030, 2018
https://doi.org/10.5194/acp-18-13013-2018

Atmospheric Chemistry and Physics
Open Access
EGU

Chlorine oxidation of VOCs at a semi-rural site in Beijing: significant chlorine liberation from $ClNO_2$ and subsequent gas- and particle-phase Cl–VOC production

Michael Le Breton[1], Åsa M. Hallquist[2], Ravi Kant Pathak[1], David Simpson[3,4], Yujue Wang[5], John Johansson[3], Jing Zheng[5], Yudong Yang[5], Dongjie Shang[5], Haichao Wang[5], Qianyun Liu[6], Chak Chan[7], Tao Wang[8], Thomas J. Bannan[9], Michael Priestley[9], Carl J. Percival[9,a], Dudley E. Shallcross[10,11], Keding Lu[5], Song Guo[5], Min Hu[5], and Mattias Hallquist[1]

[1]Department of Chemistry and Molecular Biology, University of Gothenburg, Gothenburg, Sweden
[2]IVL Swedish Environmental Research Institute, Gothenburg, Sweden
[3]Earth and Space Sciences, Chalmers University of Technology, Gothenburg, Sweden
[4]Norwegian Meteorological Institute, Oslo, Norway
[5]State Key Joint Laboratory of Environmental Simulation and Pollution Control, College of Environmental Sciences and Engineering, Peking University, Beijing, China
[6]Division of Environment and Sustainability, Hong Kong University of Science and Technology, Clearwater Bay, Kowloon, Hong Kong
[7]School of Energy and Environment, City University of Hong Kong, Hong Kong
[8]Department of Civil and Environmental Engineering, Hong Kong Polytechnic University, Hong Kong
[9]Centre for Atmospheric Science, School of Earth, Atmospheric and Environmental Science, University of Manchester, Manchester, UK
[10]School of Chemistry, University of Bristol, Cantock's Close, Bristol, UK
[11]Department of Chemistry, University of the Western Cape, Bellville, Cape Town, South Africa
[a]now at: Jet Propulsion Laboratory, California Institute of Technology, 4800 Oak Grove Drive, Pasadena, CA, USA

Correspondence: Michael Le Breton (michael.le.breton@gu.se)

Received: 9 January 2018 – Discussion started: 16 January 2018
Revised: 4 August 2018 – Accepted: 21 August 2018 – Published: 11 September 2018

Abstract. Nitryl chloride ($ClNO_2$) accumulation at night acts as a significant reservoir for active chlorine and impacts the following day's photochemistry when the chlorine atom is liberated at sunrise. Here, we report simultaneous measurements of N_2O_5 and a suite of inorganic halogens including $ClNO_2$ and reactions of chloride with volatile organic compounds (Cl–VOCs) in the gas and particle phases utilising the Filter Inlet for Gas and AEROsols time-of-flight chemical ionisation mass spectrometer (FIGAERO-ToF-CIMS) during an intensive measurement campaign 40 km northwest of Beijing in May and June 2016. A maximum mixing ratio of 2900 ppt of $ClNO_2$ was observed with a mean campaign nighttime mixing ratio of 487 ppt, appearing to have an anthropogenic source supported by correlation with SO_2, CO and benzene, which often persisted at high levels after sunrise until midday. This was attributed to such high mixing ratios persisting after numerous *e*-folding times of the photolytic lifetime enabling the chlorine atom production to reach 2.3×10^5 molecules cm^{-3} from $ClNO_2$ alone, peaking at 09:30 LT and up to 8.4×10^5 molecules cm^{-3} when including the supporting inorganic halogen measurements.

Cl–VOCs were observed in the particle and gas phases for the first time at high time resolution and illustrate how the iodide ToF-CIMS can detect unique markers of chlorine atom chemistry in ambient air from both biogenic and anthropogenic sources. Their presence and abundance can be explained via time series of their measured and steady-state calculated precursors, enabling the assessment of competing

OH and chlorine atom oxidation via measurements of products from both of these mechanisms and their relative contribution to secondary organic aerosol (SOA) formation.

1 Introduction

NO and NO_2 (NO_x) are important catalysts in the photochemical production of ozone (O_3) playing a significant role in the oxidation of volatile organic compounds (VOCs) and subsequently have an adverse effect on air quality. In the daytime, NO_x is primarily removed by the hydroxyl radical (OH) to form nitric acid (HNO_3), which is subsequently lost by wet deposition, becoming a major component of acid rain. At night, the OH radical is not a significant oxidant as photolysis stops, enabling the reaction between NO_2 and O_3 to form significant levels of the nitrate radical (NO_3) (Atkinson, 2000). NO_3 can accumulate at night or further react with NO_2, leading to the formation of N_2O_5 (Brown et al., 2003; Brown and Stutz, 2012). This equilibrium can lead to the reaction of NO_3 with VOCs at night forming organic nitrates or act as an important intermediate for heterogeneous reaction on aerosols as N_2O_5 produces NO_3^- and NO_2^+ in the aqueous phase (Hallquist et al., 1999, 2000; Wagner et al., 2013). In the presence of chlorine, which is assumed in models to predominantly come from sea salt (Baker et al., 2016), nitryl chloride ($ClNO_2$) can be formed and released into the gas phase from the aerosol surface (Osthoff et al., 2008). $ClNO_2$ formation thereafter acts as a nighttime radical reservoir due to its stability at night.

At sunrise, $ClNO_2$ is rapidly photolysed, liberating the highly reactive chlorine atom subsequently converting it into ClO, HOCl and $ClONO_2$ depending on the available sunlight, O_3, HO_x and NO_x levels via the following reaction pathways (R1–R11).

$$ClNO_2 + h\nu \rightarrow Cl + NO_2 \quad \text{(R1)}$$
$$Cl + O_3 \rightarrow ClO + O_2 \quad \text{(R2)}$$
$$ClO + NO_2 \rightarrow ClONO_2 \quad \text{(R3)}$$
$$ClO + HO_2 \rightarrow HOCl + O_2 \quad \text{(R4)}$$
$$ClONO_2 + h\nu \rightarrow Cl + NO_3 \quad \text{(R5)}$$
$$ClONO_2 + h\nu \rightarrow ClO + NO_2 \quad \text{(R6)}$$
$$HOCl + h\nu \rightarrow Cl + OH \quad \text{(R7)}$$
$$ClONO_2 + H^+ + Cl^- \rightarrow Cl_2 + HNO_3 \quad \text{(R8)}$$
$$HOCl + H^+ + Cl^- \rightarrow Cl_2 + H_2O \quad \text{(R9)}$$
$$ClO + NO \rightarrow Cl + NO_2 \quad \text{(R10)}$$
$$OH + HCl \rightarrow Cl + H_2O \quad \text{(R11)}$$

The liberated chlorine will predominantly react with VOCs, with the pathways listed (Reactions R2–R11) representing alternative routes to loss of the chloride radical, and contribute to daytime photochemical oxidation, competing with OH and perturbing standard organic peroxy radical abundance (RO_x = OH + HO_2 + RO_2), O_3 production rate, NO_x lifetime and partitioning between reactive forms of nitrogen (Riedel et al., 2014). The rate constants for the reaction of chlorine atoms with a number of VOCs is around 200 times larger than the equivalent reaction with OH (Tanaka et al., 2003); therefore, its abundance, fate and cycling can significantly alter standard daytime oxidation pathways. The oxidation of VOCs by chlorine atoms is thought to be significant in the early hours of the day while OH mixing ratios are low and chlorine atom production is high through the photolysis of $ClNO_2$, as well as feeding into the standard HO_x / NO_x cycles via production of peroxy radicals from reactions with alkanes. Additional Cl_2 photolysis and HCl reaction with OH can also produce chlorine atoms throughout the day but at lower rates.

Saturated hydrocarbons are usually oxidised by reaction with OH or a chlorine atom to form an organic peroxy radical (RO_2), and H_2O or HCl depending on the oxidant (Reactions R12 and R13), which is the dominant pathway for chloride–VOC (Cl–VOC) reactions. In a heavily polluted environment such as Beijing, the RO_2 favours further reactions with NO to form an oxygenated volatile organic compound (HO_2 and NO_2) or an alkyl nitrate ($RONO_2$). Specifically, acyl peroxy radicals can also react with NO_2 to form acyl peroxy nitrates (APNs) such as peroxy acetyl nitrate (PAN).

$$RH + OH \xrightarrow{O_2} RO_2 + H_2O \quad \text{(R12)}$$
$$RH + Cl \xrightarrow{O_2} RO_2 + HCl \quad \text{(R13)}$$

$$RO_2 + NO \rightarrow OVOC + HO_2 + NO_2 \quad \text{(R14a)}$$
$$RO_2 + NO \rightarrow RONO_2 \quad \text{(R14b)}$$

$$RO_2 + NO_2 \leftrightarrow APN \quad \text{(R15)}$$

Addition of the chlorine atom to an unsaturated VOC can also occur and then continue on the similar reaction pathway as denoted by Reactions (R12)–(R15). These pathways result in the production of unique chlorine atom chemistry markers which have been previously investigated to indicate the extent of chlorine atom oxidation reactions (Riemer et al., 2008; Keil and Shepson, 2006). The utilisation of these compounds, such as 2-chloro-peroxypropionyl nitrate (2-Cl PPN) and 1-chloro-3-methyl-3-butene-2-one (CMBO), as chlorine atom chemistry markers relies on the abundance of the chlorine atom, the VOC precursor, HO_x, NO_x and O_3 and competing pathways for chlorine atom reactions. Riedel et al. (2014) calculated that up to 10 parts per trillion (ppt) Cl–VOCs are formed as a result of chlorine atom addition to alkenes and can therefore provide a number of potential periods of dominating active Cl chemistry (Wang et al., 2001).

The production of chloroperoxy radicals via chlorine atom addition can lead to the formation of semivolatile oxidation products which have been observed for both biogenic (Cai and Griffin et al., 2008) and anthropogenic emissions (Huang

et al., 2014; Riva et al., 2015) in controlled laboratory studies. Chlorine-initiated oxidation of isoprene could also represent a significant oxidation pathway due to its rapid reaction rate compared with OH (Orlando et al., 2003) resulting in gas-phase products such as chloroacetaldehyde and CMBO, a unique tracer for atmospheric chlorine atom chemistry (Nordmeyer et al., 1997). Furthermore, reactions of the chlorine atom with isoprene or its secondary organic aerosol (SOA) derived products could serve as an atmospheric chlorine sink (Ofner et al., 2012). D. Wang et al. (2017) revealed chlorine-initiated oxidation of isoprene can produce SOA yields up to 36 %, with products similar to that of OH isoprene oxidation, compared with the 15 % yield from standard oxidation calculated by Liu et al. (2016), although this is known to be a factor of 2 higher than utilised in standard climate models. This SOA formation from chlorine-initiated oxidation presents a large knowledge gap in the literature, which to date is limited by measurement capabilities.

This complex system results in a large uncertainty in the global budget of chlorine atoms of $\sim$ 15–40 Tg Cl yr^{-1} calculated by indirect means (Allan et al., 2007; Platt et al., 2004), which is further limited by the ability of measurement techniques to accurately quantify short-lived species at low mixing ratios. Our knowledge of the Cl budget therefore depends on the accurate measurement of its precursors, namely $ClNO_2$ and major reaction pathways of the chlorine atom upon liberation in the daytime. Measurements to date show that the mixing ratio of $ClNO_2$ vary geographically from below limits of detection to hundreds of ppt (Mielke et al., 2015; Phillips et al., 2012; Bannan et al., 2015) and up to 3 parts per billion (ppb) (Tham et al., 2014; Riedel et al., 2014; Liu et al., 2017) in heavily polluted urban areas. To date, the majority of these measurements have been performed in the United States, with more recent research in Europe, China, etc. (Tham et al., 2014; Wang et al., 2016; X. Wang et al., 2017; Z. Wang et al., 2017; Liu et al., 2017). A major factor in the variation of $ClNO_2$ mixing ratios is the availability and abundance of aerosol chloride which can vary significantly, although it is predominantly present as sodium chloride from sea salt.

Iodide adduct ionisation has previously been applied to measure inorganic halogens in ambient air (Osthoff et al., 2008; Riedel et al., 2012; Thornton et al., 2010; Le Breton et al., 2017) using mass spectrometers with quadrupole mass analysers. This technique involves periodically changing the tuning of the spectrometer to allow transmission of a particular mass ion to the detector. Several species are therefore often "chosen" for detection in order to achieve high-enough time resolution. Recent developments and availabilities of a time-of-flight chemical ionisation mass spectrometer (ToF-CIMS) have enabled the simultaneous measurement of all detectable ions by an ionisation technique via high-frequency full mass spectral collection. The high resolving power (3500) of this technique also enables much lower limits of detection for species which may have the similar mass to a compound that is much more abundant via multi-peak fitting. This technique has previously been applied for the measurement of $ClNO_2$ and Cl_2 (Faxon et al., 2015) and recently for Cl–VOCs (D. Wang et al., 2017) in the gas phase. In this study, a ToF-CIMS utilising the Filter Inlet for Gas and AEROsols (FIGAERO) is deployed at a site in semi-rural Beijing, China, to measure the gas- and particle-phase precursors ($ClNO_2$, N_2O_5) and selective halogen-containing species at high time frequency and resolving power to further our understanding of the chlorine atom budget in this region and its potential fate.

2 Experimental

2.1 Site description

The data presented here were collected during the inter-collaborative field campaign, within the framework of a Sino-Swedish research project ("Photochemical Smog in China") aimed to further our understanding of the episodic pollution events in China through gas- and particle-phase measurements with numerous analytical instruments. The laboratory setup on the Changping University campus of Peking University was situated at a semi-rural site 40 km northwest of Beijing close to Changping (40.2207° N, 116.2312° E). The general setup has previously been described by Le Breton et al. (2018).

All instruments sampled from inlets set up in a laboratory 12 m high from 13 May to 23 June 2016. The site has a small town within its vicinity and some small factories within 5 km. A high-resolution time-of-flight aerosol mass spectrometer (HR-ToF-AMS) was utilised to measure the mass mixing ratios and size distributions of nonrefractory species in submicron aerosols, including organics, sulfate, ammonium and chloride (DeCarlo et al., 2006; Hu et al., 2013). The setup of this instrument has been previously described by Hu et al. (2016). Photolysis rates were measured by a commercial spectroradiometer for O_3, NO_2, HCHO, HONO and H_2O_2 (Metcon UF CCD); the instrument was calibrated by a high-power halogen lamp after the field campaign. The photolysis rates of other related species were scaled by the recommendation of the Jet Propulsion Laboratory (JPL) kinetic evaluation report (Burkholder et al., 2015). Before the campaign, the instrument was calibrated through comparison with a chemical actinometer utilised in 2014 (Zou et al., 2016), agreeing within 10 %. The surface albedo is normally 0.05 at the ground near the site. Upwelling radiation is neglected as is represents an insignificant fraction of the downwelling values.

An Ionicon Analytik high-sensitivity proton transfer mass spectrometer (PTR-MS) as described by de Gouw and Warneke et al. (2007) provided supporting precursor VOC measurements. Detailed information about the PTR-MS measurements can be found in Yuan et al. (2012, 2013). In

brief, 28 masses are measured throughout the campaign at 1 Hz. Zero air, which was produced by ambient air passing through a platinum catalytic converter at 350 °C (Shimadzu Inc., Japan), was measured for 15 min every 2.5 h to determine the background. Aromatic masses (m/z 79 for benzene, m/z 93 for toluene, m/z 105 for styrene, m/z 107 for C8 aromatics and m/z 121 for C9 aromatics), oxygenated masses (m/z 33 for methanol, m/z 45 for acetaldehyde, m/z 59 for acetone, m/z 71 for methyl vinyl ketone plus methacrolein and m/z 73 for methyl ethyl ketone), isoprene (m/z 69) and acetonitrile (m/z 42) were calibrated by using EPA TO15 standard from Apel-Riemer Environmental Inc., USA. Formic acid (m/z 47), acetic acid (m/z 61), formaldehyde (m/z 31) and monoterpenes (m/z 81 and m/z 137) were calibrated by permeation tubes (VICI, USA). The uncertainties of most species are below 10 %, which is detailed in the previous work (Liu et al., 2015).

2.2 ToF-CIMS setup

Gas- and particle-phase ambient species were measured using an iodide ToF-CIMS (resolving power of 3500) coupled to the FIGAERO inlet (Lopez-Hilfiker et al., 2014). The setup for this campaign has previously been described by Le Breton et al. (2018). Briefly, the iodide ionisation scheme was utilised to acquire non-fragmented ions of interest by passing ultra-high-purity N_2 over a permeation tube containing liquid CH_3I (Alfa Aesar, 99 %) and through a Tofwerk X-ray ion source type P (operated at 9.5 kV and 150 µA) to produce the iodide reagent ions. The ionised gas was then carried out of the ion source and into the ion-molecule reaction (IMR) chamber, which was heated to 40 °C to reduce wall loss, through an orifice (Ø = 1 µm). The inlet lines were 2 m long and composed of copper tubing (12 mm) for the aerosol inlet and Teflon tubing (12 mm) for the gas sample line. Particles were collected onto a Zefluor® polytetrafluoroethylene membrane filter at the same rate as the gas inlet line sampling (2 slm). FIGAERO was operated in a cyclic pattern; 25 min of gas-phase measurement and simultaneous particle collection, followed by a 20 min period during which the filter was shifted into position over the IMR inlet and the collected particle mass was desorbed.

2.3 Calibration

In the field, formic acid calibrations were performed daily, utilising a permeation source maintained at 40 °C. A dry N_2 flow (200 sccm) was passed over the permeation source and joined a 2 slm N_2 flow line directed towards the inlet. The mixing ratio of the flow was determined by mass loss in the laboratory after the campaign. The sensitivity of the ToF-CIMS to formic acid was found to be 3.4 ion counts per ppt Hz^{-1} for 1×10^5 iodide ion counts.

N_2O_5 was synthesised by mixing 20 ppm O_3 with pure NO_2 (98 %, AGA gas) in a glass vessel and then passing the mixture through a cold trap held at −78.5 °C by dry ice. The N_2O_5 was transferred to a diffusion vial fitted with a capillary tube (i.d. 2 mm). The N_2O_5 diffusion source was held at a constant temperature (−23 °C), and the mass loss rate was characterised gravimetrically for a flow rate of 100 sccm. The same flow was added to a dry nitrogen inlet dilution flow of 2 slm to calibrate the CIMS. $ClNO_2$ measurements were quantified by passing the N_2O_5 over a wetted NaCl bed to produce $ClNO_2$. The decrease in N_2O_5 from the reaction with NaCl was assumed to be equal to the mixing ratio of $ClNO_2$ produced (i.e. a 100 % yield). Conversion of N_2O_5 to $ClNO_2$ can be as efficient as 100 % on sea salt, but it can also be lower, for example, if $ClNO_2$ were to convert to Cl_2 (Roberts et al., 2008). For NaCl, the conversion efficiency has however been as low as 60 % (Hoffman et al., 2003). In this calibration, we have followed the accepted methods of Osthoff et al. (2008) and Kercher et al. (2009) that show a conversion yield of 100 % and have assumed this yield in the calibrations of this study. The lower detection limit of the CIMS to N_2O_5 and $ClNO_2$ was found to be 9.5 and 1.2 ppt, respectively, for 1 min averaged data. The error in the individual slope of the calibration results yields a total uncertainty of 30 % for both N_2O_5 and $ClNO_2$. These sensitivities for N_2O_5 and $ClNO_2$ (9.8 and 1.6 ion counts per ppt Hz^{-1} for 1×10^5 iodide ion counts) were applied relatively to that of formic acid. The other inorganic halogens reported in this work are reported in ion counts. Other acids identified by CIMS which are reported in the literature are given the sensitivity of N_2O_5 to provide a minimum concentration so no concentrations are overestimated.

A post campaign calibration of chloroacetic acid (99 %, Sigma Aldrich) was utilised to characterise a sensitivity factor for a Cl–VOC. The calibration was performed using the same method as for formic acid and gave a sensitivity of 1.02 ion counts ppt^{-1} Hz when normalised to 1×10^5 I^- ion counts. This similar sensitivity to that of the Cl–VOC to that of $ClNO_2$ could imply a relative sensitivity may be appropriate to constrain the mixing ratios of all Cl–VOCs, although further work is required to confirm this, and therefore the paper reports all Cl–VOC measurements in units of ion counts.

2.4 Model setup

The European Monitoring and Evaluation Programme (EMEP) Meteorological Synthesizing Centre – West (MSC-W) chemical transport model (Simpson et al., 2012, 2017) driven by meteorology from the Weather Research and Forecasting Advanced Research (WRF-ARW) model (Skamarock et al., 2008) was utilised to support source analysis of the particulate chloride. The model was run on two nested domains (0.5 and 0.1667° resolution, respectively) with biomass burning emissions from the two databases, the Fire Inventory from NCAR (FINN) and Global Fire Assimilation System (GFAS), and anthropogenic emissions from the Multi-resolution Emission Inventory for China (MEIC;

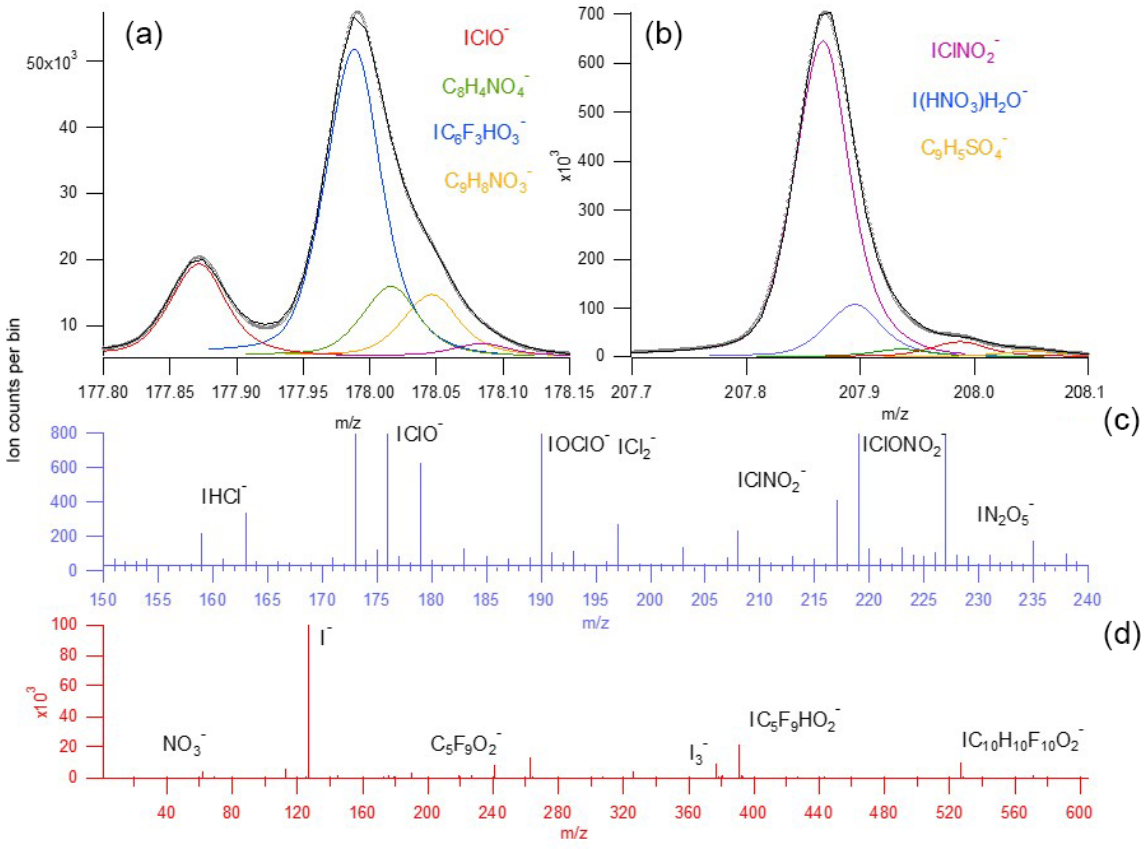

Figure 1. **(a)** Average mass spectrum for the whole measured range. **(b)** Average mass spectrum for the region that contains all gas-phase nighttime species utilised in this work. A high-resolution spectral fit for ClO and $ClNO_2$ is displayed with corresponding multi-peaks with 0.5 atomic mass units (AMU) (**c** and **d**). The black line represents the total fit from all peaks. The grey line represents the mass spectral raw data.

http://meicmodel.org/, last access: 1 March 2018). Two versions of the model, one getting emissions from open biomass burning from FINN (Wiedinmyer et al., 2011) and one getting them from GFAS (Kaiser et al., 2012), were run for the entire period of the Changping measurement campaign.

3 Results and discussion

3.1 Peak identification and quantification

Peak fitting was performed utilising the Tofware peak fitting software for molecular weights up to 620 AMU. The standard peak shape was fitted a peak on the spectra until the residual was less than 5 %. Each unknown peak was assigned a chemical formula using the peak's exact mass maxima to five decimal places and also isotopic ratios of subsequent minor peaks. An accurate fitting was characterised by a ppm error of less than 5 and subsequent accurate fitting of isotopic peaks. The analysis here focuses on species identified in the mass spectra considered to possibly play important roles with respect to the nighttime chlorine reservoir and several other key nighttime oxidants: $ClNO_2$, HCl, Cl_2, ClO, HOCl, OClO, $ClONO_2$, N_2O_5 and Cl–VOCs. Figure 1 displays the average mass spectra for the measurement campaign and the peak fitting applied for ClO and $ClNO_2$. All species were represented by a dominant peak with a multi-peak fit, although a number of coexisting peaks were present for much of the campaign. This signifies the importance of high-resolution fit data and the need for high-resolution measurements. A quadrupole CIMS may not be able to resolve the peak adjacent to ClO at m/z 178 (dominant peak is $IC_6F_3HO_3^-$) and the second dominant peak for the $ClNO_2$ fit (cluster of HNO_3 with water) would result in a 10 % overestimation.

3.2 N_2O_5 measurements

The CIMS and a cavity enhanced absorption spectrometer (CEAS) measured N_2O_5 (H. Wang et al., 2017) simultaneously from 13 May 2016 to 6 June 2016. However, given the use of FIGAERO, the CIMS alternated measurements between gas and particle phases and thus did not generate a completely continuous gas-phase time series.

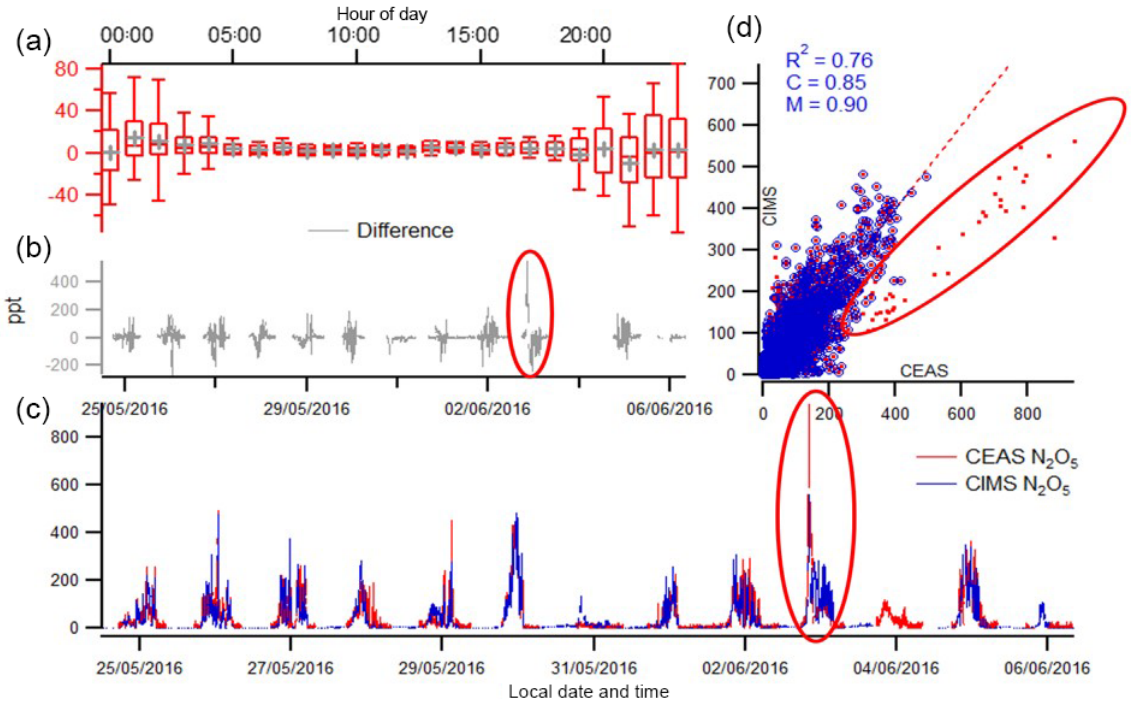

Figure 2. CIMS and cavity enhanced absorption spectrometer (CEAS) 1 min averaged data of N_2O_5 with corresponding correlation plot **(a)**, campaign and diurnal deviation (panels **b** and **c**, respectively). The red highlighted periods represent data collected on 3 June where a different correlation gradient was observed between CIMS and CEAS. The box-and-whisker plot represents the diurnal difference for the campaign between the CEAS and CIMS measurements **(d)**. Panel **(c)** shows the y intercept of the line of best fit and M is the gradient.

Here, the CEAS is utilised to validate the CIMS N_2O_5 (at m/z 235) measurements and also instrument stability. The CEAS utilised a dynamic source by mixing NO_2 and O_3 to generate stable N_2O_5 for calibration (H. Wang et al., 2017). The source was used to calibrate the ambient sampling loss of N_2O_5 in the sampling line, filter, the pre-heater cavity and optical cavity. This was performed pre- and post-campaign. During the campaign, the reflectivity of the high-reflectivity mirror was calibrated daily and the filter changed hourly. The simultaneous measurements of N_2O_5 can be shown in Fig. 2 for 1 min averaged data. The time series shows good agreement for both background mixing ratios during the day (below 10 ppt) and high nighttime mixing ratios (up to 800 ppt), excluding one night. The highest N_2O_5 levels observed by both the CEAS and CIMS were observed on 3 June, although the CEAS reports 880 ppt, whereas the CIMS reports 580 ppt. If included in the analysis, the R^2 is 0.71 and when excluded it is 0.76. To date, the reason for this deviation during that night is not known, but it should be stressed that N_2O_5 measurements are delicate and highly dependent on sampling condition, e.g. the RH. Nevertheless, excluding this night from the comparison, a slope of 0.85 is observed and an offset of 0.9 ppt. The diurnal profile in Fig. 2 represented the difference between the two measurements throughout the campaign. The largest error between the two measurements occurs at night during the higher levels of N_2O_5, although averaging at 4 ppt (representing 11 % error on the average campaign concentration). Differences could arise from a number of various factors. Inlet differences such as the CIMS-heated IMR (to 40 °C to reduce wall loss), residence time and ambient NO_2 can all change thermal decomposition and wall loss rates between the instruments, which is determined for the CEAS in H. Wang et al. (2017) but not for the CIMS in this work. Also, the separate inlets were facing in different directions within the same laboratory, possibly enabling local wind patterns to affect the mixing ratios reaching each instrument.

The CEAS data were further utilised to assess any sensitivity changes for the CIMS that daily carboxylic acid calibrations did not account for. A time series of hourly factor differences between the CIMS and CEAS was implemented into these data to weight the measurements to a normalised sensitivity. The high level of agreement (R^2 of 0.76) from low mixing ratio measurements and a species with a short lifetime from different inlets confirms the accuracy and reliability of the CIMS measurements for this campaign.

Generally, N_2O_5 was detected throughout the campaign with a clear diurnal variation peaking at night and rapidly falling to below limits of detection in the daytime as a result of photolysis of N_2O_5 and NO_3. The campaign mean nighttime mixing ratio was 121 ppt with a standard deviation of 76 ppt. The maximum mixing ratio of N_2O_5 ob-

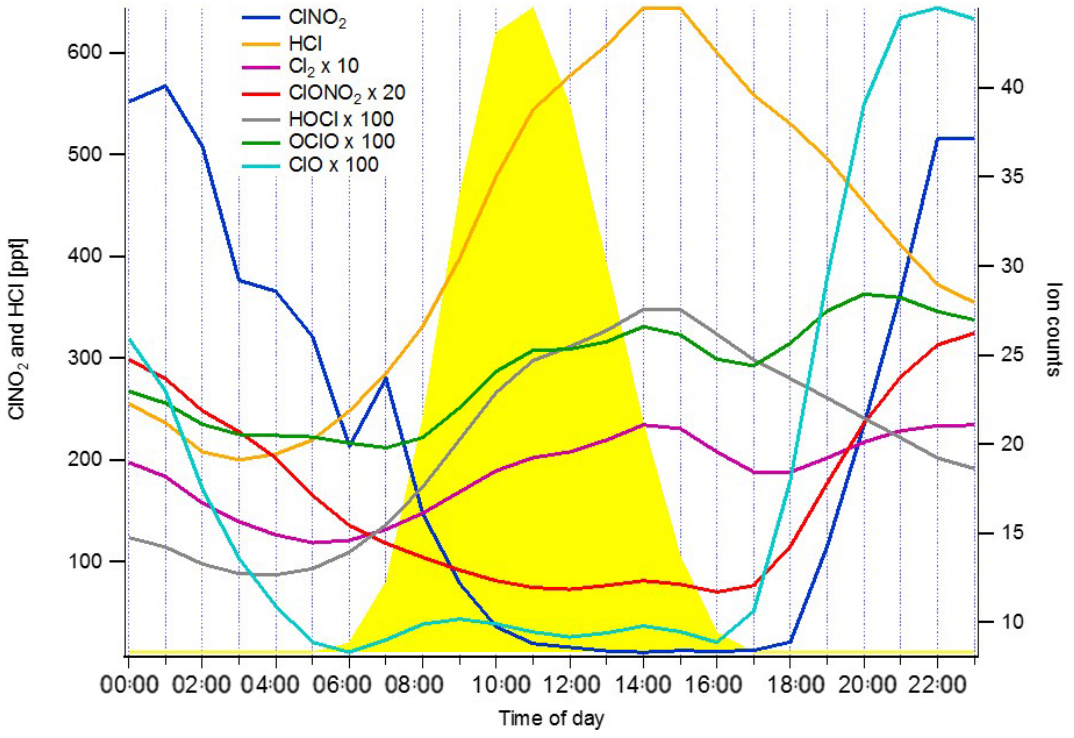

Figure 3. Mean diurnal profiles of the inorganic halogens detected by the CIMS from the 23 May to 6 June with average J rate for $ClNO_2$ as guide for photolysis. $ClNO_2$ and HCl mixing ratios are on the left y axis and the other inorganic halogens on the right y axis displayed in ion counts.

served was 880 ppt on 3 June. This range of mixing ratios lies within the recently reported values in the literature but not at the extreme mixing ratios as observed in Germany (2.5 ppb) (Phillips et al., 2016) or Hong Kong (7.7 ppb) by Wang et al. (2016). Although the mean mixing ratios do not increase significantly during the pollution episodes, the maximum mixing ratios detected overnight increase by up to a factor of 4. Further analysis of N_2O_5 nighttime chemistry was performed by Wang et al. (2018), who calculated an average steady-state lifetime of 310 ± 240 s and mean uptake coefficient of 0.034 ± 0.018.

3.3 Inorganic chlorine: abundance, profiles and source

3.3.1 Abundance and profiles

Mean diurnal profiles of HCl, Cl_2, $ClONO_2$, HOCl, ClO and $ClNO_2$ are displayed in Fig. 3 from data between 23 May and 6 June. HCl exhibited a standard diurnal profile increasing in mixing ratio throughout the day and peaking at 16:00 LT which then fell off slowly at night. The mean HCl campaign mixing ratio was 510 ppt (standard deviation (σ) 270 ppt) and the maximum HCl mixing ratio was 1360 ppt on 30 June. Cl_2 exhibited a diurnal profile peaking in both nighttime and daytime. High mixing ratios were observed at night followed by a sharp loss at sunrise and a general build-up throughout the day. The campaign mean mixing ratio was 0.65 ppt (σ 0.5 ppt) and the maximum mixing ratio was 4.2 ppt on 4 June just before midnight. This agrees well with recent urban measurements of Cl_2 in the US where Faxon et al. (2015) observed a maximum of 3.5 ppt and Finley et al. (2006) observed up to 20 ppt in California. Up to 500 ppt Cl_2 have recently been reported in the Wangdu County, southwest of Beijing (Liu et al., 2017). Although the mixing ratios we report here are significantly lower, as detailed later, their source may be of similar origin, which is indicated to be from power plant emissions.

The diurnal profile of HOCl peaked during the daytime via its main formation pathways via reaction of ClO and HO_2 and Cl with OH. Interestingly, the ClO in this work exhibits a nighttime diurnal peak, contradicting known formation pathways via Cl reaction with O_3 and the photolysis of $ClONO_2$. The complexity continues as $ClONO_2$ also peaks during the night, given that its main known formation pathway is via reaction of ClO (produced at sunrise via $ClNO_2$ photolysis) with NO_2. The misidentification of $ClONO_2$ and ClO is not thought to be a possible reason for these discrepancies due to the low number of mass spectral peaks that have maxima at night and the mass defect of chlorine making the peak position unique to chlorine-containing molecules. IMR chemistry is also not a possible source as these reactions would occur throughout the day, therefore skewing all of the data and not just the nighttime levels, although there is a possibility that

$ClONO_2$ can be formed in the IMR by reactions between ClO and NO_2. It is hypothesised that in extremely high OH and HO_2 mixing ratios, all ClO is rapidly converted to HOCl, limiting the formation on significant levels of ClO and subsequently $ClONO_2$. Khan et al. (2008) suggest that Cl atoms of around 2×10^4 molecules cm^{-3} could be present at night via analysis of alkane relative abundance. Although a formation mechanism is not proposed, it provides further evidence that ClO formation at night is possible and may represent an unknown reaction pathway, which would agree with the measurements presented in this work.

$ClNO_2$ exhibited a similar diurnal profile as N_2O_5, peaking at night and lost during daylight due to photolysis. The campaign mean nighttime mixing ratio was 487 ppt. The maximum mixing ratio observed was 2900 ppt on 31 May, similar to that previously measured at semi-rural site in Wangdu (up to 1500 ppt) (Liu et al., 2017), Mount Tai (2000 ppt) (Z. Wang et al., 2017), but lower than that in Hong Kong (4 ppb) (Wang et al., 2016).

3.3.2 Source of chloride

The high levels of $ClNO_2$ indicate a local significant source of chlorine to support these observations. The dominant source of chlorine atoms for $ClNO_2$ production within models, such as the Master Chemical Mechanism (MCM), is from sea salt. However, the site is situated 200 km from the Yellow Sea, and therefore this origin would have a low probability. The mean AMS chloride mass loading was 0.05 $\mu g\,m^{-3}$ for the campaign with a maximum of 1.7 $\mu g\,m^{-3}$. The Cl^- from the AMS appears to be correlated strongly with CO and SO_2, possibly originating from power plants or combustion sources. It should be noted that the AMS data do not include refractory aerosol and also have a cut-off size larger than the anticipated size of sea salt particles. Instead, the high Cl^- observed appears to originate from mainland areas to the site (Fig. 4) rather from the nearest coast, further supporting a anthropogenic source. Tham et al. (2016) observed a strong correlation of aerosol chloride with SO_2 and potassium from measurements done during the same season in 2014 in Wangdu (a semi-rural site 160 km southwest of Beijing) and suggested contributions to fine chloride from burning of coal and crop residues. The latter was also supported by satellite fire spot count data (Tham et al., 2016). Riedel et al. (2013) have previously reported high $ClNO_2$ mixing ratios observed from urban and power plant plumes measuring high mixing ratios of gas-phase Cl_2. The correlation with SO_2 indicates coal burning as a potential source of particulate chlorine which is known to be a significant source of PM in the Beijing region (Ma et al., 2017), and the correlation with CO and benzene could be an indicator of biomass burning (Wang et al., 2002). To support this analysis, Fig. S1 in the Supplement displays a wind rose plot in which radial and tangential axes represent the wind direction and speed ($km\,h^{-1}$). The colour bar represents the $PM_{2.5}$ concentration. We could see that during the campaign, the severe pollution was from the south and southwest, with little contribution from the east part. Therefore, it is likely that little contribution of the chloride was from the ocean.

In order to test the hypothesis of biomass burning as a source of particulate chlorine, biomass burning emissions and transport utilising the EMEP MSC-W chemical transport model driven by meteorology from the WRF-ARW model (Skamarock et al., 2008) were used. Neither of the two biomass burning databases used (FINN and GFAS) contained data on chlorine emissions, so instead the biomass burning emissions of CO (CObb) were tracked and compared with the total mixing ratio of CO (COt) at the Changping site. CO was chosen since the measurements in Changping had shown a strong correlation between CO and $ClNO_2$ and because CO could be expected to be co-emitted with chlorine for both biomass burning and industrial combustion.

Figure S2 (the Supplement) shows the time series of the measured $ClNO_2$ mixing ratios at the Changping site, as well as the modelled mixing ratios of COt and CObb. CObb is shown for calculations using either the FINN or the GFAS database, while for clarity the COt is only shown using the FINN database. It is clear that mixing ratios of CObb are very low compared with COt (Fig. S2 in the Supplement). The two pollution episodes on 18–23 May and 28 May–5 June are to some extent visible in all time series, but for the biomass burning CO series the second episode is much less pronounced. Nighttime averages of the mixing ratios shown in Fig. S2 in the Supplement were calculated for each night for the time period 18:00–08:00 LT (UTC + 8), roughly corresponding to the period when $ClNO_2$ is not destroyed by photolysis. Nights with a significant amount of missing data for the measurements were excluded. Figure S2 in the Supplement shows scatter plots of these averages of $ClNO_2$ against the averages of the other species including their linear fits. The R^2 values for these fits were 0.48, 0.04 and 0.21 for COt, CObb FINN and CObb GFAS, respectively. The fact that mixing ratios of CObb are so much smaller than COt according to the model, combined with the much better correlation for COt than for CObb, strongly suggests that industrial emissions are the dominant source of chlorine, rather than biomass burning. To further investigate the source of chloride, the model was also run to calculate sea salt levels instead of CO. This resulted in a poor correlation between sea salt and the $ClNO_2$ (Fig. S4 in the Supplement). The absolute levels of sea salt calculated by the model were also very low, unlikely to be able to produce the observed mixing ratios of $ClNO_2$ as observed by CIMS.

3.4 Particle-phase $ClNO_2$

A particle desorption profile was observed in the high-resolution data for $ClNO_2$. The count increase at this 1 AMU mass can be attributed to two sources: SO_3 and $ClNO_2$ as shown in Fig. 5. The SO_3 peak is predominantly found in the

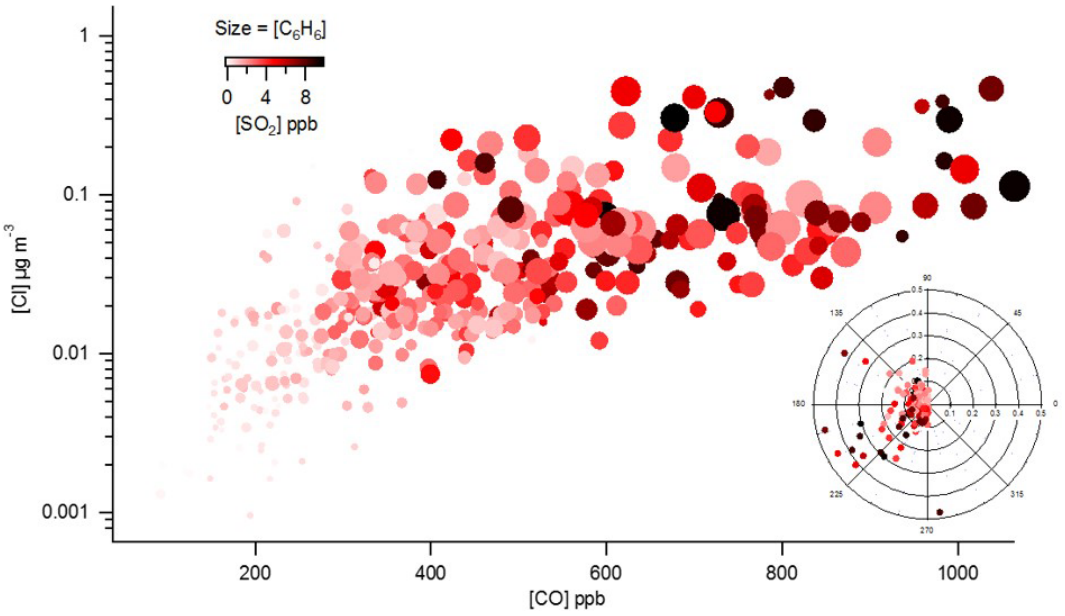

Figure 4. Correlation of particulate Cl^- from the AMS measurements and CO colour coded by the SO_2 mixing ratio and size binned by increasing benzene mixing ratio. A wind rose plot illustrates the wind direction and particulate Cl^- mixing ratio colour coded by SO_2 mixing ratio.

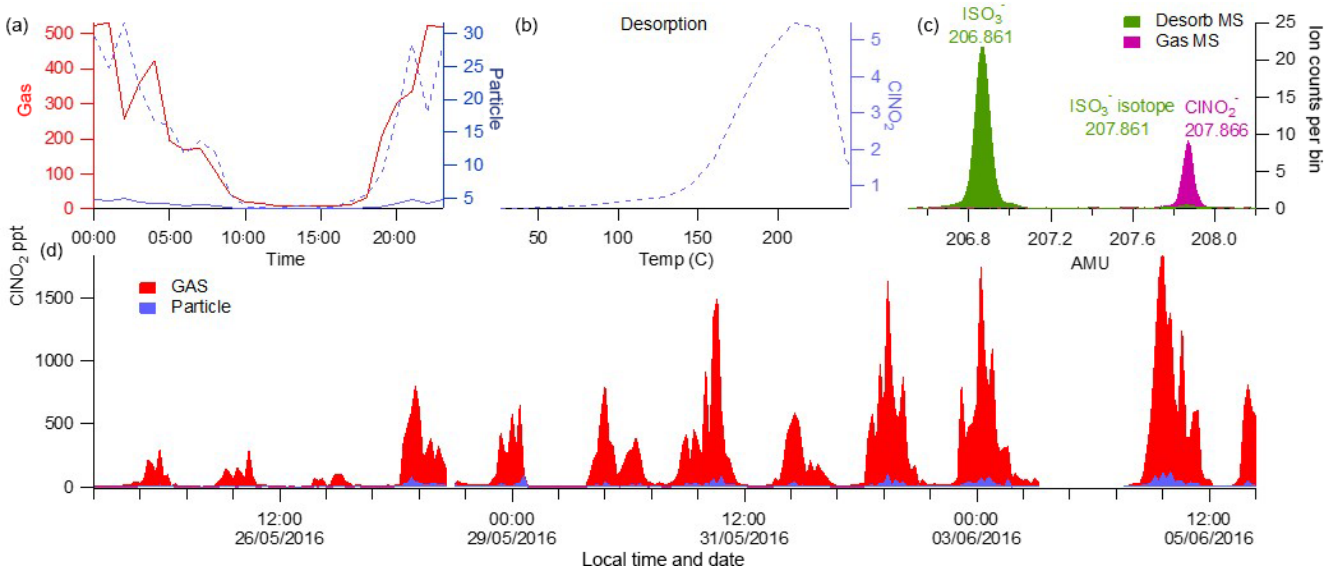

Figure 5. $ClNO_2$ gas- and particle-phase campaign time series (1 h averaged) **(a)** and average diurnal profiles **(b)**. The peak fitting for $ClNO_2$ and the SO_3 interfering mass at 207–208 AMU **(c)** and the desorption profile for the counts attributed to the high-resolution $ClNO_2$ peak **(d)**.

particle phase and is below the limit of detection (LOD) in the gas phase. During initial analysis of these data, SO_3 interfered with the $ClNO_2$ peak fitting and attributed its counts to $ClNO_2$ in the particle phase as its ^{33}S ion is only 0.005 AMU away from the $ClNO_2$ peak. Upon its inclusion into the peak list and utilisation of the Tofware feature which constrains isotopes and reallocates the signal appropriately, $ClNO_2$ remains to indicate a strong desorption profile. The diurnal cycle of this desorption correlates well with the $ClNO_2$ gas-phase profile, indicating a correct assignment of the counts to particle-phase $ClNO_2$. The desorption profiles with respect to temperature also exhibit a thermogram structure and not, for example, a gas-phase leak into the system which could have accounted for the correlation with the gas-phase time series. This suggests the possible presence of $ClNO_2$ in the particle phase. Another possible explanation could be the deposition

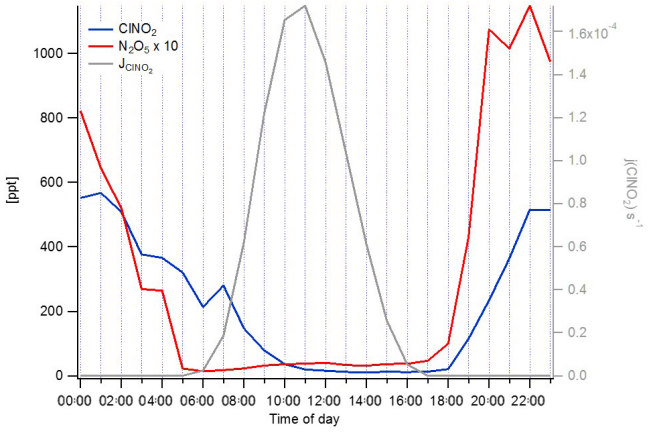

Figure 6. Diurnal profile of N_2O_5, $ClNO_2$ and $j(ClNO_2)$ for the campaign highlighting the persistence of $ClNO_2$ past sunrise and the expected rapid photolysis of N_2O_5.

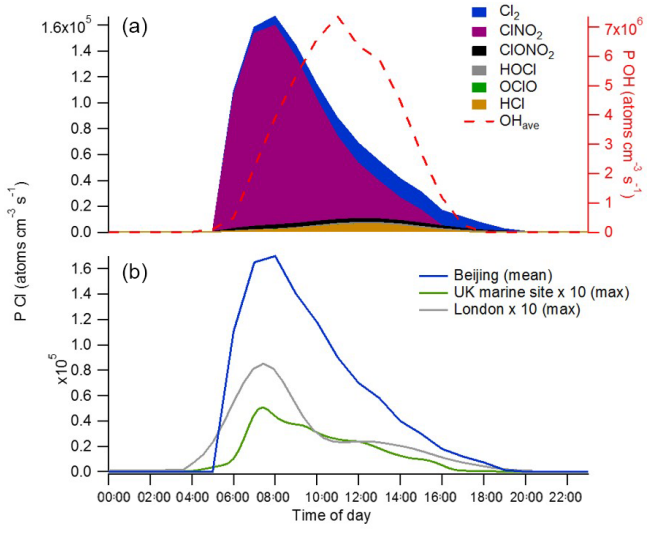

Figure 7. (a) Steady-state calculation of inorganic halogens' contribution to chlorine atom production. **(b)** Relative mean diurnal profiles of calculated chlorine atom mixing ratio calculation from this work (Beijing) and measurements in the UK (London; Bannan et al., 2015) and a marine site (Weybourne Atmospheric Observatory; Bannan et al., 2017). The steady-state OH production rate from Beijing is also displayed to illustrate relative mixing ratios of oxidants.

of $ClNO_2$ from the gas phase onto the filter as the ambient air flows through FIGAERO.

If we assume the analysis and collection technique is correct, we see an average particle- to gas-phase partitioning of 0.07, with a maximum of 0.33 and a minimum of 0.009. The average mixing ratio of $ClNO_2$ collected onto the filter during desorption is 13 ppt with a maximum of 120 ppt. Previous modelling studies assume all $ClNO_2$ is in the gas phase due to the low Henry's law constant; e.g. for the TexAQS II campaign, they calculated that 0.1 ppb in the gas phase would yield 0.54 ppt in the particle phase (Simon et al., 2009). However, these data suggest that a non-negligible amount of the chlorine associated with $ClNO_2$ is not liberated from the particle phase, assuming that no additional $ClNO_2$ is formed by thermally driven reactions. The slope of the particle- to gas-phase CIMS data is calculated to be 0.048, a factor of 96 higher than using Henry's law coefficient to estimate the particle mixing ratio.

3.5 $ClNO_2$ daytime persistence and Cl liberation

Both $ClNO_2$ and N_2O_5 are photolytically unstable, with studies reporting lifetimes on the order of hours for $ClNO_2$ depending on the solar strength (e.g. Ganske et al., 1992; Ghosh et al., 2011). Nocturnal $ClNO_2$ removal pathways have generally been reported to be negligible, with $ClNO_2$ being assumed to be relatively inert (Wilkins et al., 1974; Frenzel et al., 1998; Rossi, 2003; Osthoff et al., 2008), but the work of Roberts et al. (2008) and Kim et al. (2014) would suggest that this may not be strictly true. However, given that the average diurnal profile does not show the importance of nocturnal removal pathways in this study, observed losses are attributed solely to photolysis, with $J(ClNO_2)$ controlling the lifetime.

Rapid photolysis can be observed for N_2O_5 in Fig. 6 showing a near instant drop below LOD, whereas the $ClNO_2$ mixing ratio not only persists for up to 7 h but also shows evidence of an increase in mixing ratio at 07:00 UTC (Fig. 6). This is observed throughout the campaign and has been frequently observed in the previous study in Wangdu (Tham et al., 2016). The breakdown of the nocturnal boundary layer and inflow of air masses from above, carrying pollution from nearby industry/industries is a likely cause of this persistence of possible increase of $ClNO_2$. Liu et al. (2017) also observed high daytime mixing ratios of $ClNO_2$ (60 ppt) at the Wangdu site which they attribute to a possible oxidation mechanism due its correlation with O_3 and Cl_2 providing a daytime formation pathway to maintain mixing ratios against its rapid photolysis.

Consistent with past measurements and the measurements of this study, $ClNO_2$ is expected to provide a significant source of Cl during daytime hours, presenting a potentially significant source of the reactive Cl atom during the day. Its rapid photolysis rate and elevated mixing ratios enable Cl to compete with OH oxidation chemistry, the known dominant daytime radical source. Here, a simple steady-state calculation will be used to determine the Cl atom mixing ratio summarised as follows but detailed within the Supplement:

$$Cl_2 + h\nu \rightarrow Cl + Cl \quad \text{(ss1)}$$

$$ClNO_2 + h\nu \rightarrow Cl + NO_2 \quad \text{(ss2)}$$

$$ClONO_2 + h\nu \rightarrow ClO + NO_2 \quad \text{(ss3)}$$

$$HOCl + h\nu \rightarrow OH + Cl \quad \text{(ss4)}$$

$$OClO + h\nu \rightarrow O + ClO \quad \text{(ss5)}$$

$$OH + HCl \rightarrow Cl + H_2O \quad \text{(ss6)}$$

$$Cl + O_3 \rightarrow ClO + O_2 \quad \text{(ss7)}$$

$$Cl + CH_4 \text{ equivalent} \rightarrow HCl + \text{products} \quad \text{(ss8)}$$

$$[Cl]_{SS} = 2J_1[Cl_2] + J_2[ClNO_2] + J_3[ClONO_2] + J_4[HOCl] + J_5[OClO] + k_7[OH][HCl]\} / \{k_7[O_3] + k_8[CH_4]_{\text{equivalent}}\}, \quad \text{(ss9)}$$

where $[CH_4]_{\text{equivalent}}$ represents the reactive VOC present as if it were reacting as CH_4.

Bannan et al. (2015) were able to use this steady-state approach to compare the relative loss via reaction with OH compared with Cl atoms. Although this approach is an estimation, it was shown to produce results comparable with those of the more rigorous MCM approach, although we do acknowledge that large errors will be present in the radical species calculations, which is detailed in the supporting information. Steady-state calculations reveal a sharp rise of chlorine atoms produced at sunrise peaking at 1.6×10^5 molecules cm^{-3} around 07:00 LT which then gradually decreases, contributing to Cl atom production until 14:00 LT (Fig. 7a). Supporting Cl_2, $ClONO_2$, OClO, HOCl and HCl measurements by CIMS report that chlorine atoms can sustain a relatively high production rate until 15:00 LT as evidenced by the daytime build-up of HCl and Cl_2. $ClNO_2$ on average contributes 78 % of the chlorine atoms produced from inorganic halogens with 13 % from Cl_2. $ClNO_2$ also represents over 50 % of the chlorine atoms until midday. After approximately 15:00 LT, Cl_2 and HCl become the more dominant Cl atom sources. On the night where the highest $ClNO_2$ mixing ratios were measured, 90 % of the chlorine atoms originated from $ClNO_2$ photolysis until 14:00 LT, and HCl and Cl_2 then became main contributors until 16:00 LT (up to 80 %). $ClONO_2$, HOCl and OClO appear to be insignificant contributors to chlorine atom production throughout the campaign compared with $ClNO_2$, HCl and Cl_2.

To put these chlorine atom mixing ratios into a more global perspective, data collected by the University of Manchester from a marine site and an urban European site have been compared in Fig. 7b. Bannan et al. (2015, 2017) previously utilised a box model to calculate Cl atom mixing ratios during the campaign so that the rate of oxidation of VOCs by Cl atoms could be compared with oxidation by measured OH and measured ozone. The simple steady-state calculation described previously will be used to determine the Cl atom mixing ratio for this measurement study. The results show that both at the UK marine and urban site maximum chlorine atom mixing ratios are more than an order of magnitude lower than the mean of Beijing. It should be noted that the only source of Cl in the UK studies was $ClNO_2$, but given the dominance of $ClNO_2$ in this study, the measurements presented here suggest a high importance of the chlorine chemistry for the Asian air chemistry. Studies of chlorine radical production in Los Angeles by Riedel et al. (2012) and Young et al. (2012) indicate that the high production rate in Beijing is somewhat typical of urban sites, although HCl and $ClNO_2$ contribution to radical production is the same, whereas here we see very little chloride radical production from HCl in comparison with $ClNO_2$.

Although this study does not reach the scope of characterising O_3 and RO_x production from chlorine atom chemistry, statistics are often reported with $ClNO_2$ morning chemistry via modelling simulations, and we can put into perspective the mean and maximum mixing ratios relative to other studies. Tham et al. (2016) recorded a maximum $ClNO_2$ mixing ratio of 2070 ppt from a plume originating from Tianjin, the closest megacity to Beijing, and report a 30 % increase in RO_x production and up to 13 % of O_3 production. Liu et al. (2017) observed peak mixing ratios up to 3 ppb and similar diurnal mixing ratios which they calculated contribute to a 15 % enhancement of peroxy radicals and 19 % O_3 production. Wang et al. (2016) report up to 4.7 ppb of $ClNO_2$ in Hong Kong and calculated a maximum increase of 106 % of HO_x in the morning and an enhancement of O_3 production the next day by up to 41 %. Therefore, it is evident that this work supports similar studies in Asia that conclude that chlorine atom oxidation significantly contributes to atmospheric oxidation via RO_x and O_3 production. Although several studies have demonstrated a non-negligible impact of chlorine oxidation chemistry (e.g. Oshoff et al., 2008; Riedel et al., 2014; Sarwar et al., 2014), the impact of Cl chemistry varies significantly between various areas and atmospheric conditions; e.g. Bannan et al. (2015, 2017) deemed the impact from chlorine atom chemistry to be relatively low with respect to O_3 production and competing with OH radicals for VOC oxidation.

3.6 VOC oxidation by chlorine atoms

Steady-state calculations of OH (as described by Whalley et al., 2010) estimate that campaign average maximum mixing ratio was 7×10^6 molecules cm^3 (Fig. 7b), 6 times greater than the maximum chlorine atom mixing ratio and 14 times higher than the average chlorine atom mixing ratio. Pszenny et al. (2007) report estimated OH to chlorine atom ratios, from VOC lifetime variability relationships, of 45 to 199 along the east coast of the United States. Although the ratio appears much larger than calculated in this work, here we present not only significantly higher mixing ratios of $ClNO_2$ which appear to be a consistent conclusion from measurements in Asia, but also the chlorine within this study appears to originate from an anthropogenic origin rather than marine, possessing the ability to supply a much larger reservoir of halogens to be liberated through photolysis.

The relative oxidation rate of the chlorine atom and OH to VOCs can vary greatly. Rate coefficients for reaction of Cl atoms with some volatile organic compounds have been shown to be up to 200 times faster than the comparable reaction with OH. The ratio reported here is significantly less than this each day; Cl can subsequently dominate VOC oxi-

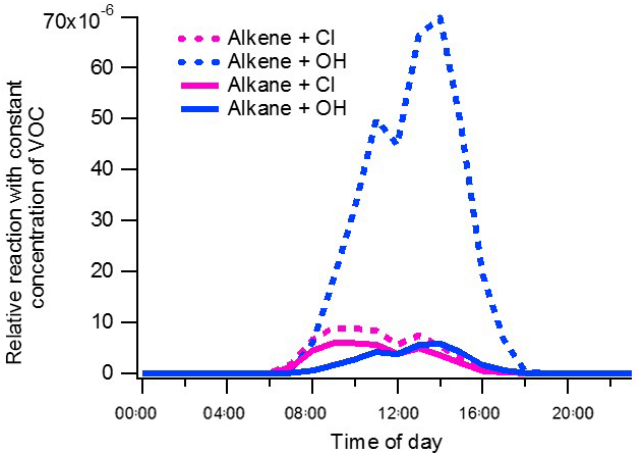

Figure 8. Mean diurnal time series of alkene (pink) and alkane (blue) relative reaction rate (arbitrary value) with the chlorine atom (dashed) and OH (solid).

dation for some fraction of the day. Here, the diurnal maxima of the chlorine atom and OH differ by 5 h, enabling chlorine atoms to dominate VOC oxidation earlier in the day before OH mixing ratios have built up. The relative oxidation rate of VOCs to OH and the chlorine atom also varies greatly, creating a difference for various VOCs. If an average reaction rate for alkenes and alkanes to Cl and OH is calculated, it is possible to generalise the significance of each oxidation pathway to qualitatively asses the contribution chlorine atoms have on oxidation chemistry. It can be seen in Fig. 8 that alkenes are much more likely to be oxidised by OH than Cl, although a significant contribution (15 %) is attributed to chlorine chemistry. Although significant if evaluated on a global level, Liu et al. (2017) estimated that Cl atoms oxidise slightly more alkanes than OH radicals in a similar region of China, implying the increased scale of chlorine oxidation in China. Alkanes are known to have a much higher Cl-to-OH relative reaction rate than alkenes, and Cl contribution to oxidation is higher than OH until midday. The contribution to oxidation remains almost equal for the remainder of the day due to the persistence of $ClNO_2$ and also relatively high levels of Cl_2 and HCl. This analysis is representative of that by Bannan et al. (2015) who report contributions of alkene and alkane oxidation by Cl up to 3 and 15 %, respectively, from $ClNO_2$ mixing ratios peaking at 724 ppt.

This significant oxidation of VOCs by chlorine atoms will result in different products to those of OH oxidation as illustrated and that neglecting the contributions made by Cl atoms will significantly underestimate the degree of chemical processing of VOCs in this study and other environments where there is a source of Cl atoms. Evidence of the proposed Cl oxidation of VOCs is validated through detection of selected Cl-induced oxidation products by the ToF-CIMS, all of which are displayed in Table 1.

3.6.1 Isoprene oxidation by the chlorine atom

1-Chloro-3-methyl-3-butene-2-one (CMBO, C_5H_6ClO), a unique marker of chlorine chemistry, has previously been measured at mixing ratios up to 9 ppt by offline gas chromatography in Houston, Texas (Tanaka et al., 2003), and in laboratory studies of chlorine–isoprene oxidation (D. Wang et al., 2017). CMBO exhibited a campaign maximum of 21 and mean of 34 ion counts (near similar ppt mixing ratio if the chloroacetic acid calibration sensitivity is applied) exhibiting a near-typical diurnal profile with abundance rising sharply after sunrise, at the same rate as the chlorine atom production, but maintaining mixing ratios past noon longer than that of isoprene and the chlorine atom.

The daily maxima of CMBO varied throughout the campaign and can be explained by the relative mixing ratios of its precursors: the chlorine atom and isoprene. Its mixing ratio throughout the campaign followed similar intensities to its precursors, and Fig. 9 highlights its dependence on both Cl atom and isoprene mixing ratios. The production rate of Cl and mixing ratio of isoprene were relatively low from 24 to 27 May (1.6×10^5 molecules cm^{-3} s^{-1} Cl and 0.5 ppb isoprene), which resulted in relatively low CMBO mixing ratios. An increase in isoprene and Cl on 28 to 30 May was subsequently mirrored by the CMBO levels as qualitatively expected. On closer inspection of 30 and 31 May, the mixing ratio of CMBO was lower than expected on 30 May due to higher chlorine atom and isoprene mixing ratios compared with 31 May. This could be explained by anticipated higher OH mixing ratio as calculated by the steady-state model, which is also further represented by higher mixing ratios of IEPOX (isoprene epoxydiol, i.e. OH oxidation products) on 30 May. This illustrates how the ToF-CIMS can identify isoprene oxidation products of two competing oxidation pathways. The high levels of IEPOX on 28 May can also possibly describe the relatively high levels of CMBO in the particle phase due to an already well-oxidised air mass. CMBO may also not be unique to only isoprene–chloride reactions and therefore have alternative sources not represented in this data set.

Further daily oxidation rates can be probed via analysis of the related isoprene oxidation products observed by the CIMS. Figure 10 depicts the diurnal time series of the precursor itself and several Cl–VOC products and IEPOX. CMBO mixing ratios rise rapidly after sunrise due to the low mixing ratio of OH and high production rate of the chlorine atom. The secondary and tertiary products, $C_5H_9ClO_2$ and $C_5H_9ClO_3$ (also measured in the laboratory by D. Wang et al., 2017), increased in mixing ratio at a much slower rate but appear to peak later in the day (16:00 LT), whereas CMBO peaked around 10:00 LT (similar to the $ClNO_2$ peak time) and fell off, due to its further oxidation to form the secondary and tertiary products. IEPOX mixing ratios increased slowly after sunrise and peaked later in the day, as expected due to the availability of OH and competition from the chlorine

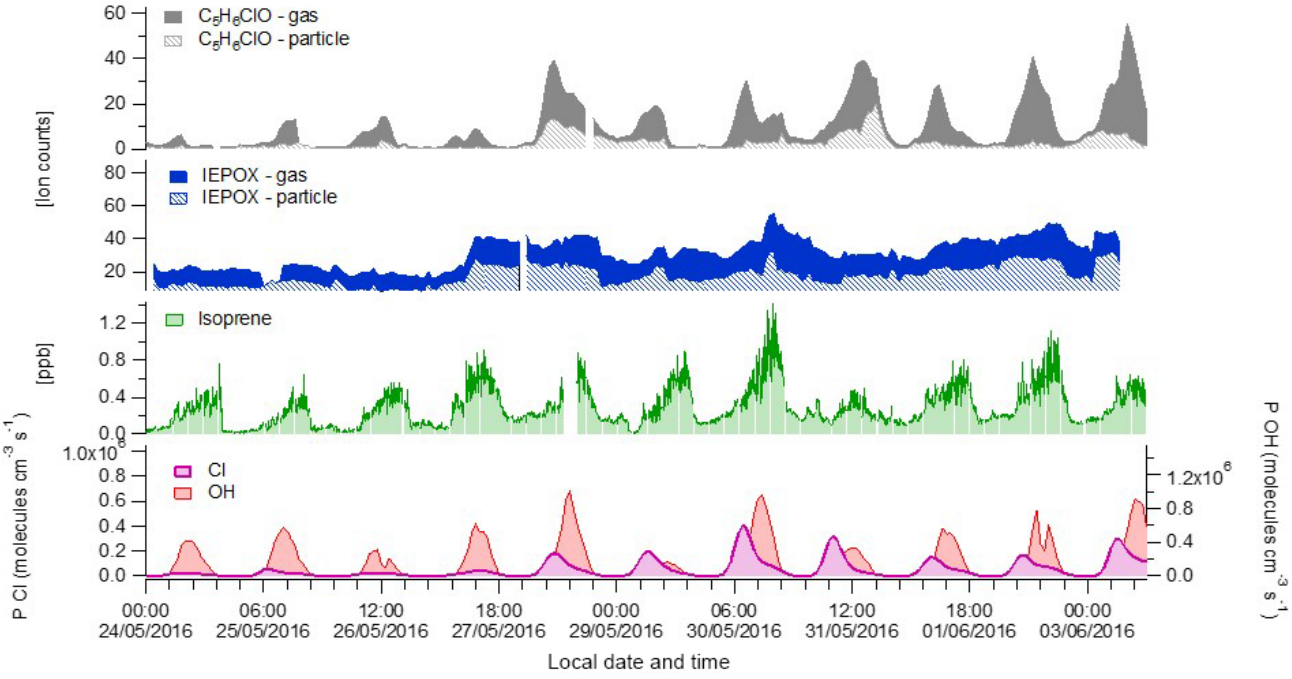

Figure 9. Campaign time series of isoprene, isoprene epoxydiol (IEPOX), CMBO and steady-state production rate of chlorine atoms and OH.

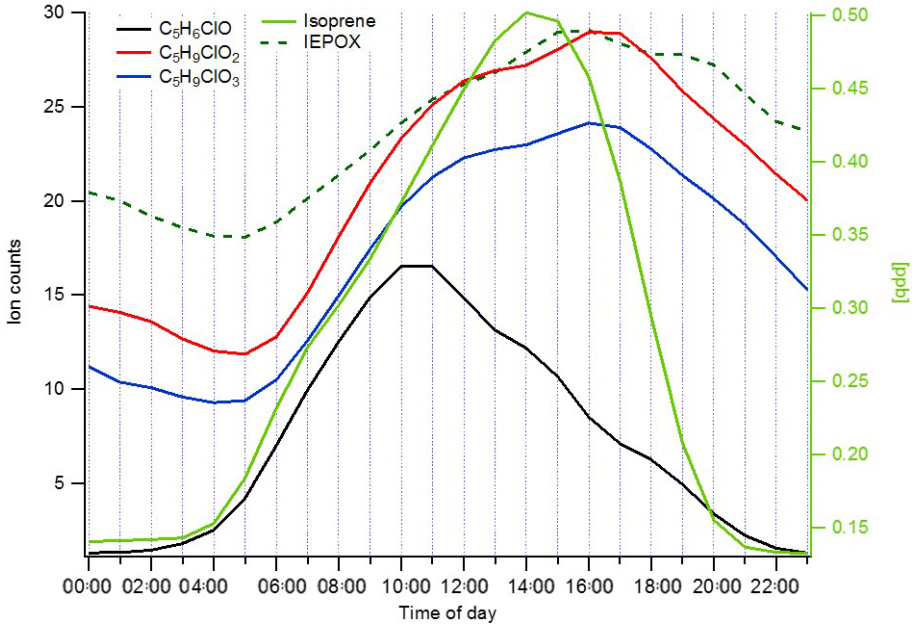

Figure 10. Mean diurnal profiles of isoprene (right *y* axis) and its OH oxidation product (IEPOX) and chlorine atom oxidation products CMBO, $C_5H_9ClO_2$ and $C_5H_9ClO_3$ (left *y* axis).

atom chemistry. The similar time series of the secondary and tertiary products to IEPOX were also reported by D. Wang et al. (2017) and were suggested to be ideal tracers of SOA production.

3.6.2 Anthropogenic Cl–VOC production

A similar unique chlorine oxidation marker in urban coastal areas, has been reported in the literature for 1,3-butadiene: 4-chlorocrotonaldehyde (CCA) (Wang et al., 2000). No mea-

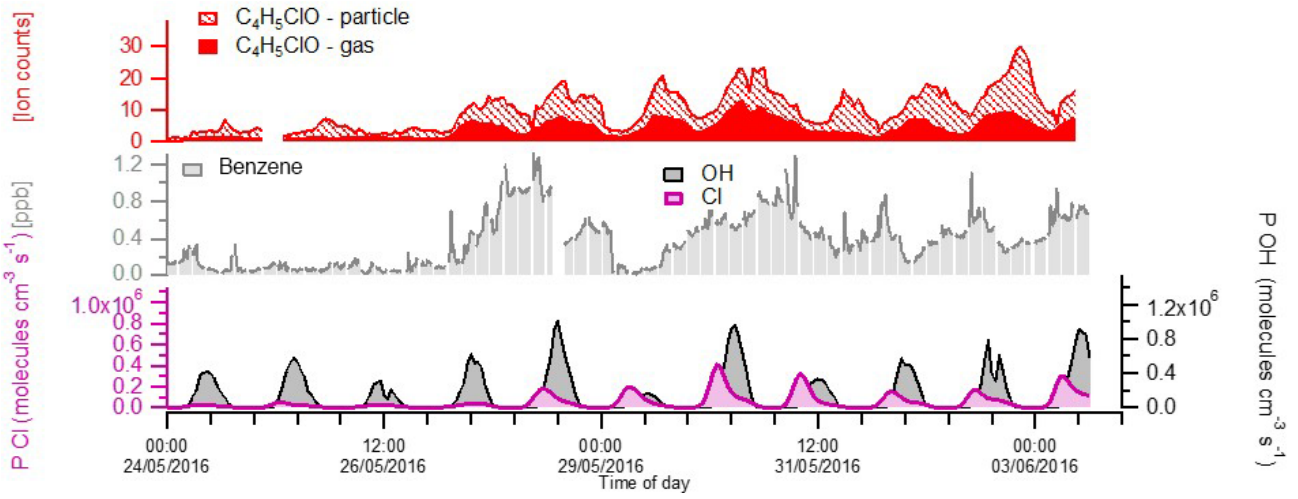

Figure 11. Campaign time series of benzene and 4-chlorocrotonaldehyde (CCA) with supporting calculations of OH and the chlorine atom production rates.

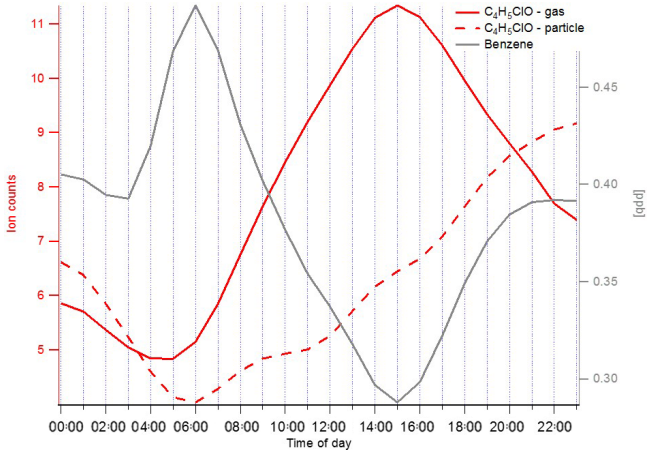

Figure 12. Mean campaign diurnal profiles of benzene (grey) and CCA in the particle (dashed red) and gas phases (solid red).

surements of 1,3-butadiene were made during this field campaign, although due to its common source to benzene (automobile exhausts (Ye et al., 1998), we present a comparison of the CCA measured by CIMS and benzene measurements made by the PTR-MS. The intensity of CCA in both the gas and particle phases reflects well the abundance of its precursors. The maximum mixing ratio of the chlorine atom coincides with a high mixing ratio of benzene and subsequently CCA on 30 May, whereas very low levels of CCA were observed for the beginning of the campaign (Fig. 11).

The diurnal time series of benzene (Fig. 12) indicates high mixing ratios in the early hours of the day, possibly associated with high anthropogenic activity or an inflow of urban air masses from downtown Beijing. The mixing ratio falls off throughout the day and almost perfectly anti-correlates with the CCA gas-phase diurnal profile which increases from sunrise and peaks at 15:00 LT. The particle-phase CCA diurnal time series steadily builds up throughout the day and does not peak until late in the evening, providing evidence of SOA production from the chlorine oxidation of anthropogenic pollutants.

Table 1. Identified Cl–VOC reaction products, nomenclature of Cl–VOC and precursor compound.

Cl–VOC	Potential nomenclature	Precursor
CHClO	formyl chloride	formaldehyde
C_2H_3ClO	chloroacetaldehyde	acetaldehyde
$C_3H_5ClNO_5$	chloro PPN	PPN
$C_3H_5ClNO_5$	chloro PAN	PAN
C_3H_5ClO	chloroacetone	acetone
$C_2H_3ClO_2$	chloroacetic acid	acetic acid
$CHClO_2$	chloroformic acid	formic acid
C_4H_7ClO	chloromethyl vinyl ketone or butanal	isoprene
C_5H_6ClO	CMBO – chloro-3-methyl-3-butene-2-one	isoprene
$C_5H_9ClO_2$	–	isoprene
$C_5H_9ClO_3$	–	isoprene
C_3H_5ClO	propanoyl chloride	1,3-butadiene
C_8H_9Cl	chloroethyl benzene	aromatic

4 Conclusions

A FIGAERO ToF-CIMS was utilised in Beijing to assess the liberation of chlorine atoms via inorganic halogen photolysis. A suite of inorganic halogens was detected, namely $ClNO_2$, reaching mixing ratios up to 2900 ppt, which is suggested to have an anthropogenic origin due to the particulate chlorine correlation with SO_2, benzene and CO. $ClNO_2$ was identi-

fied in the particle phase at higher ratios with respect to its gas-phase component than expected, which may only prove to be significant at such elevated mixing ratios as observed in east Asia. $ClNO_2$ mixing ratios above LOD persisted up to 7 h past sunrise, attributed to the lifetime of $ClNO_2$ at these high mixing ratios and a possible inflow of heavily polluted air masses from the downtown urban area. Supporting Cl_2 and HCl mixing ratios proved to be significant contributors to chlorine atom production via steady-state calculations. Compared with data attained from European-based campaigns, these mixing ratios exceed marine and urban environments by at least an order of magnitude.

This high mixing ratio of chlorine atoms resulted in a steady-state calculated OH : Cl ratio down to a factor of 6, suggesting Cl chemistry may be able to dominate alkane oxidation until midday but contribute significantly to alkene oxidation throughout the day (15 % on average). This enabled significant mixing ratios of Cl–VOCs to be formed, providing the first ambient high-time-resolution measurements of specific Cl–VOC species simultaneously measured in the gas and particle phases. The measured unique markers of chlorine chemistry for both biogenic and anthropogenic precursors provide quantitative and qualitative data to probe the extent of chlorine atom chemistry and how they compete with OH. Simultaneous measurements of the VOC precursors via PTR-MS, and IEPOX, Cl–VOCs with the CIMS provides rich information on SOA formation pathways via both OH and chlorine atom oxidation. Multistep oxidation products of Cl–VOCs were also identified and can provide partitioning information and SOA formation rates and lifetimes.

The results highlight deficiency in chlorine atom chemistry descriptions within models possibly due to a lack in quantification and identification of Cl–VOC products in the gas and particle phases. This work provides instrumental capability to probe the competition between OH and Cl oxidation chemistry and quantify their effect on ozone and SOA formation.

Data availability. The data are to be uploaded to the following server https://snd.gu.se/sv (last access: 20 August 2018).

The Supplement related to this article is available online at https://doi.org/10.5194/acp-18-13013-2018-supplement.

Author contributions. MaH, ÅMH, RKP, MiH, and SG were the project leaders for this measurement campaign. MLB and YujW operated the CIMS. QL and CKC led PAM operation and analysis. TJB, DT, and CJP led the steady sate analysis. JJ and DS led with the modelling. MG, YucW, and JY supported organosulfate analysis. DS, WZ, MP and SL supported with AMS analysis. KL supported with general data analysis and project management.

Competing interests. The authors declare that they have no conflict of interest.

Acknowledgements. The work was carried out under the framework research program on "Photochemical smog in China" financed by the Swedish Research Council (639-2013-6917). The National Natural Science Foundation of China (21677002) and the National Key Research and Development Program of China (2016YFC0202003) also helped fund this work.

Edited by: Steven Brown
Reviewed by: two anonymous referees

References

Allan, W., Struthers, H., and Lowe, D. C.: Methane carbon isotope effects caused by atomic chlorine in the marine boundary layer: Global model results compared with southern hemisphere measurements, J. Geophys. Res., 112, https://doi.org/10.1029/2006JD007369, 2007.

Baker, A. K., Sauvage, C., Thorenz, U. R., van Velthoven, P., Oram, D. E., Zahn, A., Bernninkmeijer, C. A. M., and Williams, J.: Evidence for strong, widespread chlorine atom chemistry associated with pollution outflow from continental Asia, Sci. Rep., 6, 36821, https://doi.org/10.1038/srep36821, 2016.

Bannan, T. J., Booth, A. M., Bacak, A., Muller, J. B. A., Leather, K. E., Le Breton, M., Jones, B., Young, D., Coe, H., Allan, J., Visser, S., Slowik, J. G., Furger, M., Prevot, A. S. H., Lee, J., Dunmore, R. E., Hopkins, J. R., Hamilton, J. F., Lewis, A. C., Whalley, L. K., Sharp, T., Stone, D., Heard, D. E., Fleming, Z. L., Leigh, R., Shallcross, D. E., and Percival, C. J.: The first UK measurements of nitryl chloride using a chemical ionization mass spectrometer in central London in the summer of 2012, and an investigation of the role of Cl atom oxidation, J. Geophys. Res.-Atmos., 120, 5638–5657, 2015.

Bannan, T. J., Bacak, A., Le Breton, M., Ouyang, B., Flynn, M., McLeod, M., Jones, R., Malkin, T. L., Whalley, L. K., Heard, D. E., Bandy, B., Khan, A., Shallcross, D. E., and Percival, C. J.: Ground and airborne U.K. measurements of nitryl chloride, an investigation of the role of Cl atom oxidation at Weybourne Atmospheric Observatory, J. Geophys. Res.-Atmos., 122, 11154–11165, https://doi.org/10.1002/2017JD026624, 2017.

Brown, S. S. and Stutz, J.: Nighttime radical observations and chemistry Chem. Soc. Rev., 41, 6405–6447, 2012.

Brown, S. S., Stark, H., Ryerson, T. B., et al.: Nitrogen oxides in the nocturnal boundary layer: Simultaneous, in-situ detection of NO3, N2O5, NO, NO_2 and O_3, J. Geophys. Res., 108, 4299, doi:10.1029/2002JD002917, 2003.

Brown, S. S., Dube, W. P., Tham, Y. J., Zha, Q. Z., Xue, L. K., Poon, S., Wang, Z., Blake, D. R., Tsui, W., Parrish, D. D., and Wang, T.: Nighttime chemistry at a high altitude site above Hong Kong, J. Geophys. Res.-Atmos., 121, 2457–2475, 2016.

Burkholder, J. B., Sander, S. P., Abbatt, J. P. D., Barker, J. R., Huie, R. E., Kolb, C. E., Kurylo, M. J., Orkin, V. L., Wilmouth, D. M., and Wine, P. H.: Chemical Kinetics and Photochemical Data for Use in Atmospheric Studies: Evaluation Number 18, Jet Propul-

sion Laboratory, California Institute of Technology, Pasadena, CA, 1–1392, 2015.

Cai, X., Ziemba, L. D., and Griffin, R. J.: Secondary aerosol formation from the oxidation of toluene by chlorine atoms, Atmos. Environ., 42, 7348–7359, 2008.

DeCarlo, P. F., Kimmel, J., Trimborn, A., Northway, M., Jayne, J. T., Aiken, A., Gonin, M., Fuhrer, K., Horvath, T., Docherty, K., Worsnop, D. R., and Jimenez, J. L.: Field-deployable, high-resolution, time-of-flight Aerosol Mass Spectrometer, Anal. Chem., 78, 8281–8289, 2006.

de Gouw, J. and Warneke, C.: Measurements of volatile organic compounds in the earth's atmosphere using proton-transferreaction mass spectrometry, Mass Spectrom. Rev., 26, 223–257, 2007.

Faxon, C. B., Bean, J. K., and Ruiz, L. H.: Inland Mixing ratios of Cl_2 and $ClNO_2$ in Southeast Texas suggest chlorine chemistry significantly contributes to atmospheric reactivity, Atmosphere, 6, 1487–1506, 2015.

Finley, B. D. and Saltzman, E. S: Measurement of Cl_2 in coastal urban air, Geophys. Res. Lett., 33, https://doi.org/10.1029/2006GL025799, 2006.

Hoffman, R. C., Gebel, M. E., Fox, B. S., and Finlayson-Pitts, B. J.: Knudsen cell studies of the reactions of N_2O_5 and $ClONO_2$ with NaCl: Development and application of a model for estimating available surface areas and corrected uptake coefficients, Phys. Chem. Chem. Phys., 5, 1780–1789, 2003.

Hu, W. W., Hu, M., Yuan, B., Jimenez, J. L., Tang, Q., Peng, J. F., Hu, W., Shao, M., Wang, M., Zeng, L. M., Wu, Y. S., Gong, Z. H., Huang, X. F., and He, L. Y.: Insights on organic aerosol aging and the influence of coal combustion at a regional receptor site of central eastern China, Atmos. Chem. Phys., 13, 10095–10112, https://doi.org/10.5194/acp-13-10095-2013, 2013.

Hu, W., Hu, M., Hu, W., Jiminez, J. L., Yuan, B., Chen, W., Wangm M., We, Y., Chen, C., Wang, Z., Peng, J., Zeng, L., and Shao, M.: Chemical composition, sources, and aging process of submicron aerosols in Beijing: Contrast between summer and winter, J. Geophys. Res., 121, 1955–1977, 2016.

Huang, M., Liu, X., Hu, C., Guo, X., Gu, X., Zhao, W., Wang, Z., Fang, L., and Zhang, W.: Aerosol laser time-of-flight mass spectrometer for the on-line measurement of secondary organic aerosol in smog chamber, Meas. J. Int. Meas. Confed., 55, 394–401, 2014.

Kaiser, J. W., Heil, A., Andreae, M. O., Benedetti, A., Chubarova, N., Jones, L., Morcrette, J.-J., Razinger, M., Schultz, M. G., Suttie, M., and van der Werf, G. R.: Biomass burning emissions estimated with a global fire assimilation system based on observed fire radiative power, Biogeosciences, 9, 527–554, https://doi.org/10.5194/bg-9-527-2012, 2012.

Keil, A. and Shepson, P.: Chlorine and bromine atom ratios in the springtime Arctic troposphere as determined from measurements of halogenated volatile organic compounds, J. Geophys. Res., 111, https://doi.org/10.1029/2006JD007119, 2006.

Kercher, J. P., Riedel, T. P., and Thornton, J. A.: Chlorine activation by N_2O_5: simultaneous, in situ detection of $ClNO_2$ and N_2O_5 by chemical ionization mass spectrometry, Atmos. Meas. Tech., 2, 193–204, https://doi.org/10.5194/amt-2-193-2009, 2009.

Khan, M. A. H., Ashfold, M. J., Nickless, G., Martin, D., Watson, L. A., Hamer, P. D., Wayne, R. P., Canosa-Mas, C. E., and Shallcross, D. E.: Night-time NO_3 and OH radical mixing ratios in the United Kingdom inferred from hydrocarbon measurements, Atmos. Sci. Lett., 9, 140–146, 2008.

Kim, M. J., Farmer, D. K., and Bertram, T. H.: A controlling role for the air–sea interface in the chemical processing of reactive nitrogen in the coastal marine boundary layer, P. Natl. Acad. Sci. USA, 111, 2943–3948, 2014.

Le Breton, M, Bannan, T. J., Shallcross, D. E., Khan, M. A., Evans, M. J., Lee, J., Lidster, R., Andrews, S., Carpenter, L., Schmidt, J., Jacob, D., Harris, N. R. P., Bauguitte, S.-J., Gallagher, M., Bacak, A., Leather, K. E., and Percival, C. J.: Enhanced ozone loss by active inorganic bromine chemistry in the tropical troposphere, Atmos. Environ., 155, 21–28, 2017.

Le Breton, M., Wang, Y., Hallquist, Å. M., Pathak, R. K., Zheng, J., Yang, Y., Shang, D., Glasius, M., Bannan, T. J., Liu, Q., Chan, C. K., Percival, C. J., Zhu, W., Lou, S., Topping, D., Wang, Y., Yu, J., Lu, K., Guo, S., Hu, M., and Hallquist, M.: Online gas- and particle-phase measurements of organosulfates, organosulfonates and nitrooxy organosulfates in Beijing utilizing a FIGAERO ToF-CIMS, Atmos. Chem. Phys., 18, 10355–10371, https://doi.org/10.5194/acp-18-10355-2018, 2018.

Le Breton, M., Hallquist,Å. M., Pathak, R. K., Simpson, D., Wang, Y., Johansson, J., Zheng, J., Yang, Y., Shang, D., Wang, H., Liu, Q., Chan, C., Wang, T., Bannan, T. J., Priestley, M., Percival, C. J., Shallcross, D. E., Lu, K., Guo, S., Hu, M., and Hallquist, M.: Datasets, https://snd.gu.se/sv, last access: 20 August 2018b.

Liu, Y., Yuan, B., Li, X., Shao, M., Lu, S., Li, Y., Chang, C.-C., Wang, Z., Hu, W., Huang, X., He, L., Zeng, L., Hu, M., and Zhu, T.: Impact of pollution controls in Beijing on atmospheric oxygenated volatile organic compounds (OVOCs) during the 2008 Olympic Games: observation and modeling implications, Atmos. Chem. Phys., 15, 3045–3062, https://doi.org/10.5194/acp-15-3045-2015, 2015.

Liu, J., D'Ambro, E. L., Lee, B. H., Lopez-Hilfiker, F., Zaveri, R. A., RiveraRios, J. C., Keutsch, F. N., Lyer, S., Kurtne, T., Zhang, Z., Gold,A., Surratt, J. D., Shilling, J. E., and Thornton, J. A.: Efficient Isoprene Secondary Organic Aerosol Formation from a Non-IEPOX Pathway, Environ. Sci. Technol., 50, 9872–9880, 2016.

Liu, M. X., Song, Y., Zhou, T., Xu, Z. Y., Yan, C. Q., Zheng, M., Wu, Z. J., Hu, M., Wu, Y. S., and Zhu, T.: Fine particle pH during severe haze episodes in northern China, Geophys. Res. Lett., 44, 5213–5221, https://doi.org/10.1002/2017GL073210, 2017.

Lopez-Hilfiker, F. D., Mohr, C., Ehn, M., Rubach, F., Kleist, E., Wildt, J., Mentel, Th. F., Lutz, A., Hallquist, M., Worsnop, D., and Thornton, J. A.: A novel method for online analysis of gas and particle composition: description and evaluation of a Filter Inlet for Gases and AEROsols (FIGAERO), Atmos. Meas. Tech., 7, 983–1001, https://doi.org/10.5194/amt-7-983-2014, 2014.

Ma, Q., Shuxiao, S. C., Zhao, B., Martin, R. V., Brauer, M., Cohen, A., Jiang, J., Zhou, W., Hao, J., Frostad, J., Forouzanfar, M. H., and Burnett, T.: Impacts of coal burning on ambient PM_1 pollution in China, Atmos. Chem. Phys., 17, 4477–4491, https://doi.org/10.5194/acp-17-4477-2017, 2017.

Mielke, L. H., Furgeson, A., Odame-Ankrah, C. A., and Osthoff, H. D.: Ubiquity of $ClNO_2$ in the urban boundary layer of Calgary, AB, Canada, Canadian J. Chem., 414–423, https://doi.org/10.1139/cjc-2015-0426, 2015.

Nordmeyer, T., Wang, W., Ragains, M. L., Finlayson-Pitts, B. J., Spicer, C. W., and Plastridge, R. A.: Unique products of the re-

action of isoprene with atomic chlorine: Potential markers of chlorine atom chemistry, Geophys. Res. Lett., 24, 1615–1618, https://doi.org/10.1029/97GL01547, 1997.

Ofner, J., Balzer, N., Buxmann, J., Grothe, H., Schmitt-Kopplin, P., Platt, U., and Zetzsch, C.: Halogenation processes of secondary organic aerosol and implications on halogen release mechanisms, Atmos. Chem. Phys., 12, 5787–5806, https://doi.org/10.5194/acp-12-5787-2012, 2012.

Orlando, J. J., Tyndall, G. S., Apel, E. C., Riemer, D., and Paulson, S. E.: Rate coefficients and mechanisms of the reaction of Cl-atoms with a series of unsaturated hydrocarbons under atmospheric conditions, Int. J. Chem. Kinet., 35, 334–353, 2003.

Osthoff, H. D., Roberts, J. M., Ravishankara, A. R., Williams, E. J., Lerner, B. M., Sommariva, R., Bates, T. S., Coffman, D., Quinn, P. K., and Dibb, J. E.: High levels of nitryl chloride in the polluted subtropical marine boundary layer, Nat. Geosci., 1, 324–328, 2008.

Phillips, G. J., Tang, M. J., Thieser, J., Brickwedde, B., Schuster, G., Bohn, B., Lelieveld, J., and Crowley, J. N.: Significant mixing ratios of nitryl chloride observed in rural continental Europe associated with the influence of sea salt chlorine and anthropogenic emissions, Geophys. Res. Lett., 39, L10811, https://doi.org/10.1029/2012GL051912, 2012.

Phillips, G. J., Thieser, J., Tang, M., Sobanski, N., Schuster, G., Fachinger, J., Drewnick, F., Borrmann, S., Bingemer, H., Lelieveld, J., and Crowley, J. N.: Estimating N_2O_5 uptake coefficients using ambient measurements of NO_3, N_2O_5, $ClNO_2$ and particle-phase nitrate, Atmos. Chem. Phys., 16, 13231–13249, https://doi.org/10.5194/acp-16-13231-2016, 2016.

Platt, U., Allan, W., and Lowe, D.: Hemispheric average Cl atom concentration from $^{13}C/^{12}C$ ratios in atmospheric methane, Atmos. Chem. Phys., 4, 2393–2399, https://doi.org/10.5194/acp-4-2393-2004, 2004.

Pszenny, A. A. P., Fischer, E. V., Russo, R. S., Sive, B. C., and Varner, R. K.: Estimates of Cl atom mixing ratios and hydrocarbon kinetic reactivity in surface air at Appledore Island, Maine (USA), during International Consortium for Atmospheric Research on Transport and Transformation/Chemistry of Halogens at the Isles of Shoals, J. Geophys. Res., https://doi.org/10.5065/D68S4MVH, 2007.

Riedel, T. P., Bertram, T. H., Crisp, T. A., Williams, E. J., Lerner, B. M., Vlasenko, A., Li, S. M., Gilman, J., de Gouw, J., Bon, D. M., Wagner, N. L., Brown, S. S., and Thornton, J. A.: Nitryl chloride and molecular chlorine in the coastal marine boundary layer, Environ. Sci. Technol., 46, 10463–10470, 2012.

Riedel, T. P., Wagner, N. L., Dube, W. P., Middlebrook, A. M., Young, C. J., Ozturk, F., Bahreini, R., VandenBoer, T. C., Wolfe, D. E., Williams, E. J., Roberts, J. M., Brown, S. S., and Thornton, J. A.: Chlorine activation within urban or power plant plumes: Vertically resolved $ClNO_2$ and Cl_2 measurements from a tall tower in a polluted continental setting, J. Geophys. Res.-Atmos., 118, 8702–8715, https://doi.org/10.1002/jgrd.50637, 2013.

Riedel, T. P., Wolfe, G. M., Danas, K. T., Gilman, J. B., Kuster, W. C., Bon, D. M., Vlasenko, A., Li, S. M., Williams, E. J., Lerner, B. M., Veres, P. R., Robert, J. M., Holloway, J. S., Lefer, B., Brown, S. S., and Thornton, J. A.: An MCM modeling study of nitryl chloride ($ClNO_2$) impacts on oxidation, ozone production and nitrogen oxide partitioning in polluted continental outflow, Atmos. Chem. Phys., 14, 3789–3800, https://doi.org/10.5194/acp-14-3789-2014, 2014.

Riemer, D. D., Apel, E. C., Orlando, J. J., Tyndall, G. S., Brune, W. H., Williams, E. J., Lonneman, W. A., and Neece, J. D.: Unique isoprene oxidation products demonstrate chlorine atom chemistry occurs in the Houston, Texas urban area, J. Atmos. Chem., 61, 227–242, 2008.

Riva, M., Healy, R. M., Flaud, P. M., Perraudin, E., Wenger, J. C., and Villenave, E.: Gas- and Particle-Phase Products from the Chlorine-Initiated Oxidation of Polycyclic Aromatic Hydrocarbons, J. Phys. Chem. A, 119, 11170–11181, https://doi.org/10.1021/acs.jpca.5b04610, 2015.

Roberts, J. M., Osthoff, H. D., Brown, S. S., and Ravishankara, A. R.: N_2O_5 oxidizes chloride to Cl_2 in acidic atmospheric aerosol, Science, 321, 1059–1059, https://doi.org/10.1126/science.1158777, 2008.

Sander, R.: Modeling atmospheric chemistry: Interactions between gas-phase species and liquid cloud/aerosol particles, Surv. Geophys., 20, 1–31, 1999.

Sarwar, G., Simon, H., Xing, J., and Mathur, R.: Importance of tropospheric $ClNO_2$ chemistry across the Northern Hemisphere, Geophys. Res. Lett., 41, 4050–4058, 2014.

Simon, H., Kimura, Y., McGaughey, G., Allen, D. T., Brown, S. S., Osthoff, H. D., Roberts, J. M., Byun, D., and Lee, D.: Modeling the impact of $ClNO_2$ on ozone formation in the Houston area, J. Geophys. Res., 114, D00F03, https://doi.org/10.1029/2008JD010732, 2009.

Simpson, D., Benedictow, A., Berge, H., Bergström, R., Emberson, L. D., Fagerli, H., Flechard, C. R., Hayman, G. D., Gauss, M., Jonson, J. E., Jenkin, M. E., Nyíri, A., Richter, C., Semeena, V. S., Tsyro, S., Tuovinen, J.-P., Valdebenito, Á., and Wind, P.: The EMEP MSC-W chemical transport model – technical description, Atmos. Chem. Phys., 12, 7825–7865, https://doi.org/10.5194/acp-12-7825-2012, 2012.

Simpson, D., Bergström, R., Imhof, H., and Wind, P.: Updates to the EMEP/MSC-W model, 2016–2017, in Transboundary particulate matter, photo-oxidants, acidifying and eutrophying components, EMEP Status Report 1/2017, The Norwegian Meteorological Institute, Oslo, Norway, available at: http://www.emep.int, 115–122, 2017.

Skamarock, W. C., Klemp, J. B., Dudhia, J., Gill, D. O., Barker, D. M., Duda, M. G., Huang, X.-Y., Wang, W., and Powers, J. G.: A Description of the Advanced Research WRF Version 3, NCAR-Tech, 113, https://doi.org/10.5065/D68S4MVH, 2008.

Tanaka, P. L., Riemer, D. D., Chang, S., Yarwood, G., McDonald-Buller, E. C., Apel, E. C., Orlando, J. J., Silva, P. J., Jimenez, J. L., Canagaratna, M. R., Neece, J. D., Mullins, C. B., and Allen, D. T.: Direct evidence for chlorine-enhanced urban ozone formation in Houston, Texas, Atmos. Environ., 37, 1393–1400, 2003.

Tham, Y., Yan, C., Xue, L., Zha, Q., Wang, X., and Wang, T.: Presence of high nitryl chloride in Asian coastal environment and its impact on atmospheric photochemistry, China Sci. Bull., 59, 356–359, https://doi.org/10.1007/s11434-013-0063-y, 2014.

Tham, Y. J., Wang, Z., Li, Q., Yun, H., Wang, W., Wang, X., Xue, L., Lu, K., Ma, N., Bohn, B., Li, X., Kecorius, S., Groß, J., Shao, M., Wiedensohler, A., Zhang, Y., and Wang, T.: Significant concentrations of nitryl chloride sustained in the morning: investigations of the causes and impacts on ozone production in a polluted re-

gion of northern China, Atmos. Chem. Phys., 16, 14959-14977, https://doi.org/10.5194/acp-16-14959-2016, 2016.

Thornton, J. A., Kercher, J. P., Riedel, T. P., Wagner, N. L., Cozic, J., Holloway, J. S., Dube, W. P., Wolfe, G. M., Quinn, P. K., Middlebrook, A. M., Alexander, B., and Brown, S. S.: A large atomic chlorine source inferred from mid-continental reactive nitrogen chemistry, Nature, 464, 271–274, https://doi.org/10.1038/nature08905, 2010.

Wagner, N. L., Riedel, T. P., Young, C. J., Bahreini, R., Brock, C. A., Dube, W. P., Kim, S., Middlebrook, A. M., Özturk, F., Robert, J. M., Russo, R., Sive, B., Swarthout, R., Thornton, J. A., VandenBoer, T. C., Zhou, Y., and Brown, S. S.: N_2O_5 uptake coefficients and nocturnal NO_2 removal rates determined from ambient wintertime measurements, J. Geophys. Res. Atmos., 118, 9331–9350, 2013.

Wang, D. S. and Ruiz, L. H.: Secondary organic aerosol from chlorine-initiated oxidation of isoprene, Atmos. Chem. Phys., 17, 13491–13508, https://doi.org/10.5194/acp-17-13491-2017, 2017.

Wang, H., Chen, J., and Lu, K.: Development of a portable cavity-enhanced absorption spectrometer for the measurement of ambient NO_3 and N_2O_5: experimental setup, lab characterizations, and field applications in a polluted urban environment, Atmos. Meas. Tech., 10, 1465–1479, https://doi.org/10.5194/amt-10-1465-2017, 2017.

Wang, T., Cheung, T., Li, Y., Yu, X., and Blake, D.: Emission characteristics of CO, NO_x, SO_2 and indications of biomass burning observed at a rural site in eastern China, J. Geophys. Res.-Atmos., 107, Pages ACH 9-1–ACH 9-10, https://doi.org/10.1029/2001JD000724, 2002.

Wang, T., Tham, Y. J., Xue, L., Li, Q., Zha, Q., Wang, Z., Poon, S. C. N., Dube, W. P., Blake, D. R., Louie, P. K. K., Luk, C. W. Y., Tsui, W., and Brown, S. S.: Observations of nitryl chloride and modeling its source and effect on ozone in the planetary boundary layer of southern China, J. Geophys. Res., 121, 2476–2489, 2016.

Wang, W. and Finlayson-Pits, B. J.: Unique markers of chlorine atom chemistry in coastal urban areas: The reaction with 1,3-butadiene in air at room temperature, J. Geophys. Res., 106, 4939–4958, 2001.

Wang, X., Wang, H., Xue, L., Wang, T., Wang, L., Gu, R., Wang, W., Than, Y. T., Wang, Z., Yang, L., Chen, J., and Wang, W.: Observations of N_2O_5 and $ClNO_2$ at a polluted urban surface site in North China: High N_2O_5 uptake coefficients and low $ClNO_2$ product yields, Amtos. Environ., 156, 125–134, 2017.

Wang, Z., Wang, W., Tham, Y. J., Li, Q., Wang, H., Wen, L., Wang, X., and Wang, T.: Fast heterogeneous N_2O_5 uptake and $ClNO_2$ production in power plant and industrial plumes observed in the nocturnal residual layer over the North China Plain, Atmos. Chem. Phys., 17, 12361–12378, https://doi.org/10.5194/acp-17-12361-2017, 2017.

Whalley, L. K., Furneaux, K. L., Goddard, A., Lee, J. D., Mahajan, A., Oetjen, H., Read, K. A., Kaaden, N., Carpenter, L. J., Lewis, A. C., Plane, J. M. C., Saltzman, E. S., Wiedensohler, A., and Heard, D. E.: The chemistry of OH and HO_2 radicals in the boundary layer over the tropical Atlantic Ocean, Atmos. Chem. Phys., 10, 1555–1576, https://doi.org/10.5194/acp-10-1555-2010, 2010.

Wiedinmyer, C., Akagi, S. K., Yokelson, R. J., Emmons, L. K., Al-Saadi, J. A., Orlando, J. J., and Soja, A. J.: The Fire INventory from NCAR (FINN): a high resolution global model to estimate the emissions from open burning, Geosci. Model Dev., 4, 625–641, https://doi.org/10.5194/gmd-4-625-2011, 2011.

Ye, Y., Galbally, I. E., Weeks, I. A., Duffy, B. L., and Nelson, P. F.: Evaporative emissions of 1,3-butadiene from petrol-fuelled motor vehicles, Atmos. Environ., 32, 2685–2692, 1998.

Young, C. J., Washenfelder, R. A., Roberts, J. M., Mielke, L. H., Osthoff, H. D., Tsai, C., Pikelnaya, O., Stutz, J., Veres, P. R., Cochran, A. K., VandenBoer, T. C., Flynn, J., Grossberg, N., Haman, C. L., Lefer, B., Stark, H., Graus, M., de Gouw, J., Gilman, J. B., Kuster, W. C., and Brown, S. S.: Vertically Resolved Measurements of Nighttime Radical Reservoirs; in Los Angeles and Their Contribution to the Urban Radical Budget, Environ. Sci. Technol., 46, 10965–10973, https://doi.org/10.1021/es302206a, 2012.

Zou, Q., Lu, K. D., Wu, Y. S., Yang, Y. D., Du, Z. F., and Hu, M.: Ambient photolysis frequency of NO_2 determined using chemical actinometer and spectroradiometer at an urban site in Beijing, Front Env. Sci. Eng., 10, 13 pp., https://doi.org/10.1007/s11783-016-0885-3, 2016.